Crystal structures of human Ero1α reveal the mechanisms of regulated and targeted oxidation of PDI

Inaba, Kenji
Division of Protein Chemistry, Post-Genome Science Center, Medical Institute of Bioregulation, Kyushu University

Masui, Shoji
Division of Protein Chemistry, Post-Genome Science Center, Medical Institute of Bioregulation, Kyushu University

Iida, Hiroka
Division of Protein Chemistry, Post-Genome Science Center, Medical Institute of Bioregulation, Kyushu University

Vavassori, Stefano
Division of Genetics and Cell Biology, Università Vita-Salute San Raffaele Scientific Institute | Division of Genetics and Cell Biology, Università Vita-Salute San Raffaele Scientific Institute

他

出版情報：The EMBO Journa. 29 (19), pp.3330-3343, 2010-09-10. European Molecular Biology Organization
バージョン：
権利関係：

Crystal structures of human Ero1α reveal the mechanisms of regulated and targeted oxidation of PDI

Kenji Inaba[1]*, Shoji Masui[1], Hiroka Iida[1], Stefano Vavassori[2], Roberto Sitia[2†] and Mamoru Suzuki[3†]

[1]*Division of Protein Chemistry, Post-Genome Science Center, Medical Institute of Bioregulation, Kyushu University, 3-1-1 Maidashi, Higashi-ku, Fukuoka 812-8582, Japan*

[2]*Università Vita-Salute San Raffaele Scientific Institute, Division of Genetics and Cell Biology, Via Olgettina 58, I-20132 Milan, Italy*

[3]*Institute for Protein Research, Osaka University, Osaka 565-0871, Japan*

[†]These two authors equally contributed to this work.

---

*Corresponding author:

Kenji Inaba; Division of Protein Chemistry, Post-Genome Science Center, Medical Institute of Bioregulation, Kyushu University, 3-1-1 Maidashi, Higashi-ku, Fukuoka 812-8582, Japan

e-mail: inaba-k@bioreg.kyushu-u.ac.jp

Tel/Fax: +81-92-642-6433

Running title: Crystal structure of human Ero1α

Precise character count of the manuscript: 52,678

Categories: Proteins, Structural Biology

Abstract

In the endoplasmic reticulum (ER) of eukaryotic cells, Ero1 flavoenzymes promote oxidative protein folding via protein disulphide isomerase (PDI), generating reactive oxygen species (hydrogen peroxide) as byproducts. Therefore, Ero1 activity must be strictly regulated to avoid futile oxidation cycles in the ER. While regulatory mechanisms restraining Ero1α activity ensure that not all PDI is oxidized, its specificity toward PDI could allow other resident oxidoreductases to remain reduced and competent to carry out isomerization and reduction of protein substrates. In this study, crystal structures of human Ero1α were solved in its hyperactive and inactive forms. Our findings reveal that human Ero1α modulates its oxidative activity by properly positioning regulatory cysteines within an intrinsically flexible loop, and by finely tuning the electron shuttle ability of the loop through disulphide rearrangements. Specific PDI targeting is guaranteed by electrostatic and hydrophobic interactions of Ero1α with the PDI b'-domain through its substrate-binding pocket. These results reveal the molecular basis of the regulation and specificity of protein disulphide formation in human cells.

Key words: disulphide bond/ ER quality control/ human Ero1α/ redox homeostasis/ X-ray crystal structure analysis

Introduction

Many secretory and membrane proteins form disulphide bonds in the endoplasmic reticulum (ER), under the assistance of numerous thiol-disulphide oxidoreductases (Appenzeller-Herzog and Ellgaard, 2008; Hatahet et al., 2009; Sevier and Kaiser, 2006). Elaborate redox-networks allow formation and isomerization of disulphide bonds until the native state is attained. The major players in oxidative reactions are protein disulphide isomerase (PDI) and Ero1, both highly conserved from yeast to mammals (Cabibbo et al., 2000; Frand and Kaiser, 1998; Mezghrani et al., 2001; Pollard et al., 1998). Ero1 generates disulphide bonds *de novo* in conjunction with a flavin adenine dinucleotide (FAD) cofactor and transfers them to PDI (Tavender and Bulleid, 2010; Tu and Weissman, 2004). PDI, an ER-resident member of the thioredoxin (Trx)-fold family, is composed of two redox-active Trx domains with a CGHC motif (a- and a'-domains), two redox-inactive Trx domains (b- and b'-domains), an additional α-helical domain (c-domain) and a linker loop (x-linker) between the b'- and a'-domains. Crystal structures of yeast PDI (Pdi1p) revealed that these domains are lined up in the order a-b-b'-a'-c, and they can assume different spatial arrangements, 'twisted U-shape' or 'boat', indicating conformational flexibility of the enzyme (Tian et al., 2008; Tian et al., 2006). Alternative conformations were also reported for human and thermophilic fungus PDIs (Nguyen et al., 2008; Serve et al., 2010; Wang C, 2010).

Since the discovery of an essential PDI-Ero1 oxidative pathway in *Saccharomyces cerevisiae*, its operation mechanisms have been studied using genetic, biochemical, and structural approaches (Sevier and Kaiser, 2008). Recent biochemical studies demonstrated that yeast Ero1 (Ero1p) preferentially oxidises the CXXC motif in the N-

terminal Trx domain (a-domain) of Pdi1p among the active sites of oxidoreductases present in the yeast ER, leading to a preferred pathway for oxidising the ER thiol pool (Vitu et al., 2010). Further, the crystal structure of Ero1p, where its N-terminal (Thr19-Thr55) and C-terminal (Asn425-Gln560) regions were removed to obtain a high-quality protein crystal, revealed the fold of its catalytic core region and the structure of the FAD-containing reaction center (Gross et al., 2004).

The generation of each disulphide bond by Ero1p can be accompanied by the production of one molecule of hydrogen peroxide (H_2O_2), a potential reactive oxygen species (ROS) source (Gross et al., 2006). While the cell can cope with peroxides formed during routine oxidative protein folding and sometimes utilizes them as a messenger in the cell-signaling cascades (Veal et al., 2007) and possibly as a direct protein disulphide introducer (Karala et al., 2009), ROS production that exceeds the capacity of the cellular antioxidant defense systems could induce harmful ER oxidative stress. Overexpression of Ero1p was shown to cause a significant increase in ROS (Haynes et al., 2004), whereas partial lowering of Ero1 activity by RNAi abrogated ROS accumulation in ER-stressed animals and enhanced resistance to the lethal effects of high levels of ER stress (Harding et al., 2003; Marciniak et al., 2004). These observations suggested that Ero1 activity must be tightly regulated in living cells. Yeast Ero1p, indeed, was found to exert an inbuilt feedback regulation mechanism, in which two non-catalytic cysteine pairs (Cys90-Cys349 and Cys150-Cys295) sense the ER redox environment: their oxidation decreases Ero1p activity, thus preventing potentially futile and cell-damaging cycles and ER hyper-oxidation (Sevier et al., 2007).

Human cells contain two Ero1 isoforms: Ero1α that is expressed in most cell types,

and Ero1β that is found only in select tissues (Dias-Gunasekara et al., 2005; Pagani et al., 2000). While these two Ero1 isoforms seem to have selective, non-redundant functions in oxidative protein folding, the disruption of both isoforms only modestly delayed IgM production, suggesting the occurrence of Ero1-independent disulphide formation pathways in mammalian cells (Zito et al., 2010). Both Ero1α and Ero1β contain two essential cysteine triads (Cys85-Cys94-Cys99 and Cys391-Cys394-Cys397 in the case of Ero1α) that are highly conserved from yeast to human (Bertoli et al., 2004). The last two cysteines in the N-terminal triad are involved in a direct interaction with PDI, while those in the C-terminal triad form an active-site disulphide near the FAD isoalloxazine ring. Thus, the Cys94-Cys99 pair functions as a shuttle disulphide, transferring reducing equivalents from PDI to the FAD-containing reaction center in Ero1α. In contrast to yeast Ero1p, human Ero1α was found to oxidise the C-terminal Trx domain (a'-domain) of human PDI more effectively than the a-domain (Baker et al., 2008; Wang et al., 2009).

In living cells, human Ero1α accumulates in two main redox isoforms with different electrophoretic mobilities on non-reducing gels (Ox1 and Ox2) (Benham et al., 2000). Recent studies showed that these redox forms reflect disulphide bond rearrangements among Cys94, Cys99, Cys104 and Cys131, and may help modulate Ero1α activity: Ox1 and Ox2 represents active and inactive states of the enzyme, respectively (Appenzeller-Herzog et al., 2008; Baker et al., 2008). However, yeast Ero1p lacks cysteine residues corresponding to Ero1α Cys104 and Cys131 (Fig. 1B). In the overall sequence, the amino acid identity between human Ero1α (468 residues) and yeast Ero1p (563 residues) is ~ 27% (128 residues) (Fig. 1A). To elucidate the different functional regulation mechanisms in these two homologous enzymes, we set out to obtain structural

information on human Ero1α.

Here we report the crystal structures of full-length human Ero1α in both its hyperactive and inactive forms, and we describe how human Ero1α limits its oxidative activity using four regulatory cysteines properly positioned within a critical loop that transfers electrons from PDI to the FAD-containing active site. Our work provides structural and further mechanistic insights into the internal disulphide rearrangement regulating Ero1α activity, originally proposed by the preceding studies (Appenzeller-Herzog et al., 2008; Baker et al., 2008). Our studies also suggest that the hydrophobic pocket in the PDI b'-domain is an essential element for the specific oxidation of PDI by Ero1α and electrostatic interactions play an auxiliary role in the functional Ero1α-PDI interplay. A detailed molecular view is presented of the regulated Ero1α catalysis of PDI oxidation.

Results

Overall structure of human Ero1α

High-quality crystals could not be obtained from recombinant wild-type human Ero1α. This was probably due to its heterogeneous configurations, as suggested by non-reducing SDS-PAGE (Supplemental Fig. S1). Therefore, mutants were produced in which two of the four regulatory cysteines were mutated to alanines, so that only one disulphide bond can be formed. Previous mutagenesis studies demonstrated that Cys94-Cys99 is the essential disulphide to directly engage in disulphide exchange with PDI, and the Cys104&131Ala mutant that homogeneously forms the Cys94-Cys99 disulphide is hyperactive (Baker et al., 2008). Accordingly, this mutant exhibited an even higher rate of

oxygen consumption (i.e., PDI oxidation) than wild-type Ero1α (Fig. 1C) and migrated as a single band with a slower electrophoretic mobility than the inactive mutant as did Ox1 of cellular Ero1α (Supplemental Fig. S1; Benham et al., 2000).

Employing this hyperactive Ero1α mutant, we obtained a well-diffracting crystal of space group *I*222 with one molecule per asymmetric unit. X-ray diffraction datasets were collected at the maximum resolution (2.35 Å) using the SPring-8 beamline BL44XU. The structural model was refined at 2.35 Å to an R-factor of 0.237 (R_{free} = 0.282) with very good stereochemistry. According to PROCHECK analysis, 99.7% of the residues were in the most favored and the allowed regions of the Ramachandran diagram, while no residues were in the disallowed region (Table I).

The entire human Ero1α chain formed a single globular domain highly rich in α-helices, in which five intramolecular disulphide bonds were identified (Cys35-48, Cys37-46, Cys85-Cys391, Cys208-Cys241, and Cys394-Cys397) (Fig. 2A and 2B). Thus, the present crystallographic study confirms the human Ero1α disulphide-bond pattern suggested by mass spectrometric analyses (Appenzeller-Herzog et al., 2008). The N-terminal segment, which had been deleted and therefore was structurally uncharacterized in the crystallographic study of yeast Ero1p (Gross et al., 2004), formed an anti-parallel β-hairpin containing the Cys35-48 and Cys37-46 disulphides (Fig. 2B). This region was located opposite to the reaction center, including the isoalloxazine ring of FAD and its proximal disulphide Cys394-Cys397 (Fig. 2A), making it unlikely that the N-terminal region is directly involved in PDI oxidation catalysis. Consistently, the removal of this region did not inhibit Ero1α oxidative activity *in vivo* (Bertoli et al., 2004).

Overall, the loop regions in human Ero1α were longer than those of yeast Ero1p. In

particular, three loop regions spanning Asp90 to Cys131 (loop A, 'regulatory loop'), Cys166 to Gln172 (loop B), and Gln212 to Glu238 (loop C) lacked electron density, probably due to their extreme flexibility (Fig. 2A). All of the regulatory cysteines were contained in loop A, and therefore their locations could not be specified in the hyperactive Ero1α. It may be that the intrinsically flexible nature of loop A is essential for electron shuttling from PDI to the FAD-proximal site of Ero1α.

Importantly, the catalytic core regions of human Ero1α and yeast Ero1p were nearly superimposable, with an average root-mean-square deviation (RMSD) for C_α atoms of 0.87Å (Fig. 2C). The four-helix bundle scaffold with an interior electron-accepting cofactor is a hallmark of disulphide bond-generating enzymes widely distributed from bacteria to eukaryotes (Inaba and Ito, 2008; Sevier et al., 2005). In contrast, there were large structural differences between human and yeast Ero1s in the other regions (Fig. 2C). Strikingly, while the 146Glu-161Ser segment in human Ero1α assumes a four-turn α-helix and lacks a disulphide bond, the corresponding region in yeast Ero1p is highly disordered and includes the Cys150-Cys295 disulphide as a regulatory switch (Fig. 2C) (Sevier et al., 2007). This structural difference most likely underlies the different regulatory mechanisms between the two Ero1s: in human Ero1α, the primary switch that shuts off the enzymatic activity is positioned at a different site as described later.

FAD-binding structure of human Ero1α

The Ero1α crystal structure provides strong evidence that a protein disulphide bond is generated *de novo* by cooperation of the Cys394-Cys397 pair and bound FAD in human cells. Previous biochemical studies on flavin-dependent sulfydryl oxidases (such as avian

egg white oxidase and augmenter of liver regeneration) have suggested that the transient formation of a charge transfer (CT) complex and a C(4a) covalent adduct between flavin and a thiolate anion of a nearby cysteine is an obligatory step for disulphide bond generation (Heckler et al., 2008). In the redox-active center of human Ero1α, the S^{γ} atom of Cys397 was separated from the flavin C(4a) atom by only 3.30 Å (Fig. 3A), a possible range for CT complex and covalent adduct formation after reduction of the Cys394-Cys397 disulphide. A chemical scheme of *de novo* disulphide bond generation by human Ero1α is therefore proposed in which Cys397 sequentially forms a CT complex and a C(4a) adduct with flavin. As a final step, Cys394 (a partner cysteine of Cys397) nucleophilically attacks the C–S bond of the adduct, yielding Cys394-Cys397 disulphide and reduced FAD ($FADH_2$) (Fig. 3C).

The FAD-binding modes of human and yeast Ero1s are remarkably similar, and involve the stacking of the Trp200 and His255 (His231 in yeast Ero1p) head groups between the isoalloxazine and adenine rings of FAD (Fig. 3B). These two aromatic residues are universally conserved in the Ero1 and Erv2 families (Fass, 2008), where Erv2 is another FAD-containing sulfydryl oxidase family first identified in the yeast ER (Sevier et al., 2001). In addition, residues that contact oxygen atoms of the pyrophosphate moiety are highly conserved among flavoenzymes (Dym and Eisenberg, 2001). Arg287 is the representative residue in human Ero1α, and appears to serve as a counter ion to the phosphate group similar to Arg260 in yeast Ero1p (Fig. 3B).

Although Ero1α consumes molecular oxygen as an electron acceptor for the catalysis of PDI oxidation, a channel or pathway for an oxygen molecule to the flavin is not evident in the structure. The FAD isoalloxazine ring was completely embedded within the

protein portion and shielded with its own dinucleotide moiety (Fig. 3D). This observation may suggest that some dynamic motion must occur for molecular oxygen to enter and reach the reaction center of Ero1α. In this context, we note that the extended loop spanning from Leu183 to Pro194 resides just above the FAD isoalloxazine ring (Fig. 3D). It will be interesting to see if the redox-dependent interplay between FAD and its neighboring polypeptide or the PDI-binding to Ero1α modulates the conformation and dynamism of the FAD-proximal region, thereby facilitating molecular oxygen entry.

Structure and function of the inactive form of human Ero1α

As addressed above, human Ero1α possesses four regulatory cysteines (Cys94, Cys99, Cys104 and Cys131), whose pairing determines its PDI oxidation activity. To elucidate the molecular mechanism underlying this functional regulation, we constructed and analyzed the crystal structure of an inactive Ero1α mutant that had both Cys99 and Cys104 mutated into alanines. As a result, this mutant is likely to homogeneously contain the Cys94-Cys131 disulphide, instead of the Cys94-Cys99 disulphide that serves as a shuttle disulphide in the hyperactive form. The extremely slow oxygen consumption of this variant confirmed its gross inactivity (Fig. 1C). Additionally, inactive Ero1α exhibited a single band with faster electrophoretic mobility on a non-reducing SDS gel (Supplemental Fig. S1), consistent with the fact that the Cys94-Cys131 disulphide bond is a peculiar feature of the Ox2 isoform (Appenzeller-Herzog et al., 2008). The crystal of the inactive Ero1α variant belongs to the space group *I*222 with one molecule per asymmetric unit, similar to the hyperactive form. The X-ray diffraction dataset was collected at the maximum resolution (3.07Å) using the SPring-8 beamline BL44XU

(Table 1).

The overall structure of the inactive form was mostly superimposable to that of the hyperactive form (Supplemental Fig. S2), indicating that no gross conformational changes occur upon rearrangement of the regulatory disulphide bonds. However, the electron density map around the regulatory loop was significantly affected by Cys94-Cys131 disulphide formation (Fig. 4A). Whereas the electron density of the hyperactive form was completely invisible for the region from Asp90 to Cys131, the inactive form exhibited a significant electron density that was derived from the Cys94-Cys131 disulphide and the polypeptide segment in front of Cys94. This was most likely due to the increased constraint caused by the disulphide linkage between Cys94 and Cys131.

One possible reason for the reduced activity imposed by the Cys94-Cys131 disulphide might be a lowered affinity with PDI. To examine this possibility, the interaction between Ero1α and PDI was analyzed by surface plasmon resonance (SPR) under a redox condition mimicking that in the ER (GSH:GSSG ratio of 4:1). A two-state model yielded the best fit and therefore was adopted to calculate the association and dissociation rate constants using the first equilibrium constants. When hyperactive Ero1α was immobilized, wild-type PDI showed rapid association (2.0×10^3 $M^{-1}s^{-1}$) and slow dissociation (4.1×10^{-3} s^{-1}) kinetics, resulting in a dissociation constant (K_D) of ~ 2.1 μM (Fig. 4C). The observed interaction is likely to reflect the reversible non-covalent association rather than the transient mixed disulphide formation, since cysteine-less PDI in which both the CXXC motifs in the a- and a'-domain were mutated to AXXA showed similar association and dissociation kinetics to wild-type PDI (Supplemental Fig. S3). Notably, the inactive Ero1α variant exhibited slightly lower affinity for PDI, with a (K_D)

of ~ 7.7 μM (Fig. 4C). The results suggest that rearrangement of the regulatory disulphides somewhat affect the PDI-binding ability of Ero1α. However, the ~3.7-fold lowered affinity alone will not be able to explain the substantial loss of function for the inactive Ero1α variant.

An alternative explanation could be that the process of electron shuttling from Cys94-Cys131 to Cys394-Cys397 is substantially prevented in the inactive Ero1α variant. The crystal structure of inactive Ero1α revealed that the sulfur atoms of Cys131 and Cys394 were separated by 12.5 Å (Fig. 4B). This geometry seems unsuitable for the intramolecular electron shuttle in Ero1α, given that the loop segment including Cys131 is not very flexible. Indeed, the region just after Cys131 assumes a short α-helix not only in the inactive but also in the hyperactive forms (Fig. 4A), suggesting that the motion of Cys131 is restricted to a certain extent even upon the cleavage of the Cys94-Cys131 disulphide.

To increase the mobility of the Cys131-neighboring region, we examined the functional effects of inserting a three- or six-glycine repeat into the site immediately after Cys131 (Fig. 5A). Despite of such engineering, these two constructs were predominantly in an oxidised form (Supplemental Fig. S1), indicating little effects of the glycine-insertion on the Cys94-Cys131 disulphide formation. Additionally, the insertions marginally affected the affinity of the inactive Ero1α variants with PDI (Supplemental Fig. S4). However, the glycine-repeat loop insertion significantly restored the PDI oxidation activity in a length-dependent manner (Fig. 5B). Thus, the restricted mobility of the Cys131-neighboring region appears to be a primary reason for the reduced activity of the mutant lacking Cys99 and Cys104.

Specific oxidation of PDI by Ero1α

Another central issue in the Ero1α-PDI oxidative axis is how Ero1α specifically and effectively oxidises PDI among the nearly twenty ER-resident PDI family member proteins (Ellgaard and Ruddock, 2005). Although human PDI and ERp57 presumably assume a similar overall fold and three-dimensional arrangement of four thioredoxin-like domains, the latter was reported to be a poor and presumably non-physiologic substrate of Ero1α (Mezghrani et al., 2001; Otsu et al., 2006). Noticeably, NMR structural analyses (Denisov et al., 2009) revealed the predominant presence of negative charges on the surface of the PDI bb'-domains; moreover, the hydrophobic pocket essential for substrate binding is located on the central cleft side of the b'-domain (Supplemental Fig. S5). In contrast, human ERp57 displays a different protein surface and electrostatic potential on its bb'-domains and lacks a substrate-binding hydrophobic pocket in the b'-domain (Kozlov et al., 2006) (Supplemental Fig. S5). Also, ERp57 bb'-domains are the minimal element sufficient for the complex formation with calreticulin (Russell et al., 2004). The sequence similarity between PDI and ERp57 is lower in the b'-domain compared to those in the a-, b-, and a'-domains (Supplemental Fig. S6), further suggesting a special role for the PDI b'-domain in binding Ero1α.

To further examine this possibility, two chimeric proteins were constructed in which the b'-domain was mutually replaced between PDI and ERp57 (Fig. 6A), and the Ero1α-catalyzed oxidation of these proteins was measured. Whereas ERp57 was a very poor substrate for Ero1α compared to PDI, the ERp57-based chimera with the PDI b'-domain was oxidised by Ero1α at a rate closer to wild-type PDI (Fig. 6B). Conversely, the PDI-

based chimera that had the ERp57 b'-domain substituted for the PDI b'-domain exhibited extremely slow oxidation by Ero1α (Fig. 6B). These results strongly suggest that the PDI b'-domain plays a critical role in the specific Ero1α catalysis of PDI oxidation.

Next, the effects of domain replacement on affinity for Ero1α were investigated by SPR (Fig. 6C). ERp57 exhibited a ~10-fold lower binding rate constant than PDI, while the dissociation rate constant was similar between PDI and ERp57. Consequently, the dissociation constant ('K_D for Ero1α') of ERp57 was ~10-fold higher than that of PDI, indicating that ERp57 has much lower affinity for Ero1α than PDI. Intriguingly, the ERp57-based chimera displayed much faster kinetics especially in the association phase than wild-type ERp57, resulting in the K_D for Ero1α value closer to that of PDI (Fig. 6C). In contrast, the PDI-based chimera showed lower association and higher dissociation rate constants than wild-type PDI (Fig. 6C), resulting in the extremely high K_D for Ero1α value. Thus, the replacement of the b'-domain between PDI and ERp57 did substantially affect the affinity for Ero1α. There is a clear correlation between the affinities for Ero1α and the Ero1α-catalysed oxidation rates of PDI, ERp57 and their chimeric proteins, implying that the differences in affinity observed by the SPR can explain the differences in reactivity with Ero1α. Taken together, we conclude that the PDI b'-domain is a key functional element that determines the affinity and the reactivity between PDI and Ero1α.

Contribution of electrostatic and hydrophobic interactions to the functional Ero1α-PDI interplay

The molecular surface features of human Ero1α revealed that a positively charged patch constituted by several basic residues including Arg83, Arg383 and Arg387 is present near

the regulatory loop (Fig. 7A and 7B). Most Ero1 family proteins conserve positively charged residues (Arg or Lys) at the corresponding positions (Cabibbo et al, 2000). To examine the functional roles of this electrostatic patch in the Ero1α-PDI interplay, we mutated the three arginines near the regulatory loop to alanine (RA) or aspartate (RD) in hyperactive Ero1α. The Ero1α variants lacking the positive residues exhibited grossly compromised activity (Fig. 7C); the functional defect was greater in the RD than in the RA variants. These variants exhibited almost the same far UV CD spectra and redox state as hyperactive Ero1α (Supplemental Fig. S7A&B) and retained the ability to oxidise DTT albeit less efficiently than hyperactive Ero1α (Supplemental Fig. S7C): collectively, these results suggest that their impaired activity reflect weakened binding to PDI rather than gross structural alterations. However, the SPR measurements revealed that both the RA and RD mutants could bind PDI with slightly weakened affinity (Supplemental Fig. S7D). Thus, the positively charged patch of Ero1α is important for effective catalysis but does not seem the primary and sole interaction site for PDI.

To gain further insights into the molecular basis of interaction between Ero1α and PDI, we investigated the role of the hydrophobic pocket in the PDI b'-domain. High salt (NaCl) concentrations did not inhibit the Ero1α-catalyzed PDI oxidation. Rather, NaCl enhanced the enzymatic activity of Ero1α (Fig. 7D), suggesting that hydrophobic interactions play a dominant role in mediating Ero1α-PDI interactions in comparison to electrostatic ones. Thus, we examined effects of amphipathic chemicals or substrate proteins known to interact with the b'-domain of PDI. Triton X-100 was previously reported to substantially decrease the interactions between the PDI b'-domain and model substrate peptides (Klappa et al., 1998). This detergent inhibited the Ero1α-catalyzed

oxidation of PDI (Fig. 7E), without significantly affecting DTT oxidation (Supplemental Fig. S8). This inhibitory effect was observed also at concentrations lower than the critical micellar concentration value (~0.01%). Similar effects were obtained with 1-anilinonaphthalene-8-sulfonate (ANS, Fig. 7F), a fluorescence probe that binds to hydrophobic patches on proteins (Streyer, 1965), *de facto* competing with Ero1 for hydrophobic pocket of PDI. Remarkably, somatostatin and mastoparan, which bind the hydrophobic pocket of the PDI b'-domain with K_D values of ~35 μM and ~130 μM, respectively (Klappa et al., 1998), also inhibited PDI oxidation in a dose-dependent manner (Fig. 7G & 7H). The greater effects of somatostatin may reflect its higher affinity for PDI. These results suggest that Ero1α competes with the model substrates for PDI binding.

Discussion

Regulatory mechanism of Ero1α oxidative activity

In all eukaryotes, the ER redox must be tightly controlled. The present work elucidates the atomic-resolution structures of full-length human Ero1α in its active and inactive forms, revealing novel insights into the mechanisms of disulphide bond formation in human cells. While human Ero1α and yeast Ero1p share a four-helix bundle scaffold in the catalytic core region, and an intramolecular disulphide shuttling mechanism, there are remarkable differences in their regulation. Thus, human Ero1α does not contain a regulatory disulphide like the one (Cys150-Cys295) that in yeast Ero1p links the nonhelical cap region containing Cys100-Cys105 (shuttle cysteines) to the helical core region containing the active site Cys352-Cys355 (see Fig. 1 and supplemental Fig. S9). It

is envisaged that reduction of the Cys150-Cys295 disulphide makes the shuttle cysteines even more mobile, thereby increasing Ero1p activity (Sevier et al., 2007). Another difference is observed in the disulphide that links the first cysteines in each active triad (Cys90-349 in yeast Ero1p and Cys85-Cys391 in human Ero1α). Loss of the Cys90-Cys349 disulphide increased yeast Ero1p activity, albeit to a lesser effect than deletion of the Cys150-Cys295 couple (Sevier et al., 2007). In contrast, the Cys85-Cys391 disulphide in human Ero1α resisted GSH-mediated reduction *in vivo* (Appenzeller-Herzog et al. 2008) and its absence resulted in severe destabilization of Ero1α structure and substantial decrease in Ero1α activity (our unpublished data; Benham et al., 2000; Bertoli et al., 2004; Tavender and Bulleid, 2010).

These features imply that human and yeast Ero1s differently modulate their oxidative activity. In place of Ero1p Cys150-Cys295, human Ero1α utilizes Cys104 and Cys131 to regulate the mobility of the electron-shuttle loop, and hence its overall activity. Our results confirm that the formation of Cys94-Cys131 and possibly Cys99-Cys104 disulphides yields an inactive form (Appenzeller-Herzog et al., 2008; Baker et al., 2008). Previous studies have suggested that Cys94 is the primary residue to form mixed disulphides with PDI (Bertoli et al., 2004). An important issue concerns the identity of the partner cysteine of Cys94 during or after the disulphide exchange with PDI. In the hyperactive form containing the Cys94-Cys99 disulphide, Cys99 is unpaired during the redox interaction with PDI and is likely located around the middle of the regulatory loop, which seems to satisfactorily fulfill the electron shuttle from Cys94-Cys99 to the active-site disulphide Cys394-Cys397. In this connection, our previous study showed that a Cys99Ala mutant displayed weak dominant negative activity in the *in vivo* oxidative

folding of JcM chains, possibly reflecting its impaired detachment from PDI (Bertoli et al., 2004). It is inferred that Cys99 contributes to promoting the resolution of the PDI–Ero1α (Cys94) mixed disulphide presumably by transferring oxidising equivalents from FAD to PDI through the redox communications between the Cys394-Cys397 and Cys94-Cys99 pairs. In contrast, Cys131 bound to Cys94 in the inactive isoform is located at the edge of the regulatory loop and juxtaposed to a short α-helix (Ala133-Leu136). The resultant restricted mobility of Cys131 most likely underlies its low efficiency of intramolecular electron transfer, due to its inability to reach the inner active site. This notion is strongly reinforced by the observation that the increased mobility of the segment by glycine-repeat insertion after Cys131 significantly restored the PDI oxidation activity of the mutant (Fig. 5B). Taken together, we propose that the oxidative activity of human Ero1α is regulated by disulphide bond rearrangements within the regulatory loop, that modulate the ability to rapidly transfer reducing equivalents from PDI to the FAD-containing active site.

It is interesting to ask how the hyperactive (Ox1) and inactive (Ox2) forms are interconverted in physiological conditions. Previous pulse-chase experiments demonstrated that the Ox2 form is intrinsically stable and predominant in living cells (Benham et al., 2000). More recently, the overexpression of wild-type PDI or cysteine-less (i. e. redox-inactive) PDI was found to markedly increase the Ox1 form (Otsu et al., 2006). Conversely, PDI knockdown clearly diminished the Ox1/Ox2 ratio of endogenous Ero1α (Appenzeller-Herzog et al., 2008). These findings suggest that PDI binding induces some conformational changes in the Ero1α regulatory loop. Disulphide rearrangement within the loop is thereby promoted, leading to the preferred occurrence of

the Ox1 form. It is conceivable that PDI acts not only as a substrate but also as a modulator that lowers the energy barrier for the Ox2-Ox1 interconversion and stabilizes Ox1 relative to Ox2. The physiological reductant essential for this disulphide rearrangement remains an important open question.

Molecular basis of the specific Ero1α-PDI oxidative pathway

Another important insight gained in this work is the molecular mechanism of effective and specific PDI oxidation by Ero1α in the ER of human cells. ERp57 has a high similarity to PDI in both amino-acid sequence (Supplemental Fig. S6) and three-dimensional structure (Dong et al., 2009) (Supplemental Fig. S5). Nevertheless, Ero1α is unable to effectively oxidise ERp57 (Fig. 6B). ERp57 forms complexes with calnexin (CNX) or calreticulin (CRT) in the ER lumen (Oliver et al., 1999). It functions as a protein disulphide isomerase or reductase for glycoproteins entering the CNX cycle, a pivotal system that assists secretory protein folding (Ellgaard et al., 1999; Oliver, 1997). Although CNX or CRT may prevent Ero1α from oxidising ERp57 in physiological conditions, we observed that ERp57 intrinsically has a low reactivity with Ero1α. Accordingly, addition of CRT did not affect the kinetics of the Ero1α-catalyzed oxidation of ER57 (data not shown).

Our protein engineering approach demonstrated that substitution of the ERp57 b'-domain with that of PDI dramatically enhanced the binding kinetics and reactivity of ERp57 against Ero1α. Thus, functional association of Ero1α with the PDI b'-domain is postulated to be necessary for effective PDI oxidation by Ero1α. Consistently, the isolated a- or a'-domain of PDI was not effectively oxidised by Ero1α (Supplemental Fig.

S10). Additionally, the PDI-based chimera with the ERp57 b'-domain markedly lost its binding activity to Ero1α (Fig. 6B). On the basis of the above findings, we hypothesized that the specific interaction between the PDI b'-domain and Ero1α plays a role in activating the oxidase, possibly by inducing some conformational changes. It is also conceivable that the b'-domain has an important role in placing the a'-domain at a suitable position for oxidization by Ero1α. In agreement with our model, recent biochemical studies have indicated that the PDI fragment composed of the b'-a' domains is the minimal element for a competent Ero1α-PDI oxidative folding pathway (Wang et al., 2009).

As suggested by the different affinity for Ero1α between PDI and ERp57, their Ero1α-binding modes would be largely different. Indeed, altering the charge distributions on Ero1α surface inhibited its functional interactions with PDI (Fig. 7C). Moreover, the effects of salt, amphipathic chemicals and PDI substrates indicate that Ero1α binds PDI through the hydrophobic pocket in the b'-domain. A possible interpretation of these findings might be that the electrostatic interaction plays an auxiliary role in guiding the active site in the PDI a'-domain to the Ero1α shuttle disulphide in the binary complex that is mainly owed to the close contacts between a portion of Ero1α and the PDI hydrophobic pocket. The inhibitory effect of a model peptide was not observed for the yeast Ero1p-PDI oxidative system (Vitu et al., 2010), which is in line with the notion that yeast Ero1p binds PDI differently from human Ero1α. Since human Ero1α and substrates seem to compete for PDI binding site in the b'-domain, oxidative protein folding in human cells likely takes place stepwise: (1) reduced PDI binds Ero1α to be oxidized; (2) oxidized PDI dissociates from Ero1α to bind substrate proteins and (3) finally PDI

introduces disulphide bonds into substrate proteins. ERp57 does not have a similar hydrophobic pocket in the b'-domain, despite it can bind a variety of proteins lacking defined secondary structure (Jessop et al., 2007). In this context, it is to be noted that overexpression or downregulation of ERp57 did not influence the Ox1/Ox2 ratio in endogenous Ero1α (Appenzeller-Herzog et al., 2008). In short, the interplay between Ero1α and PDI is extremely specific and well-tuned in living cells.

In summary, the present findings elucidate the molecular basis of regulated and specific PDI oxidation by Ero1α. The strictly defined and regulated Ero1α-PDI oxidative pathway should help prevent indiscriminate and futile electron flows in the ER environment crowded with numerous redox enzymes. Besides the potentially toxic effects of H_2O_2 generated as byproducts, an uncontrolled Ero1 activity could ultimately prevent disulphide isomerization, an essential step for proteins that fold via intermediates containing non-native disulphide bonds (Jansens et al., 2002). Structural analysis of the Ero1α-PDI complex is currently ongoing to further clarify how the two molecules interact and exchange electrons. A more precise description of the thiol-based redox networks in the ER and a comprehensive elucidation of their regulatory mechanisms would further increase our understanding of the molecular mechanisms of ER quality control, an exciting topic of study in present-day molecular cell biology.

Materials and methods

Preparation and crystallization of the hyperactive and inactive forms of human Ero1α

The cDNA encoding human Ero1α without the signal sequence was subcloned into the

*NdeI-BamH*I site of the pET15b vector (Novagen). Ero1α derivatives with site-directed Cys-to-Ala mutations in the regulatory loop were constructed using a Quik Mutagenesis Kit (Stratagene) with appropriate primer sets. Additionally, the Cys166Ala mutation was introduced into all Ero1α constructs to avoid aberrant formation of the disulphide-linked Ero1α dimer. Ero1α was overexpressed in *E. coli* strain BL21(DE3). Cells were grown at 30°C in Luria-Bertani (LB) medium containing 50 μg/ ml ampicillin and 10 μM FAD and isopropyl-β-D-thiogalactoside (IPTG) was added at a final concentration of 0.5 mM at A_{600} = ~ 0.5. After an additional 4 h of shaking, cells were harvested. The cell lysate supernatant was applied to a Ni-NTA Sepharose open column (QIAGEN). To prepare the fully oxidised form of Ero1α, potassium ferricyanide was added to the Ero1α solution at a final concentration of 20 mM, and the solution was left on ice for 20 min. The sample was then purified by size-exclusion chromatography with the Superdex 200 column (GE Healthcare). Fractions containing monomeric Ero1α species were further purified by anion exchange chromatography with a MonoQ column (GE Healthcare) (see also Supplemental Materials and Methods for more information). Recombinant Ero1α was thereafter used for functional assays, including oxygen consumption and SPR measurements. Purified Ero1α exhibits the maximum absorbance around 450 nm due to the bound FAD, and an extinction coefficient of 12.5 $mM^{-1}cm^{-1}$ at 454 nm was used to quantify the concentration of FAD-bound Ero1α (Gross et al., 2006). Determination of total protein concentration by the bicinchoninate (BCA) method revealed that our preparation of FAD-bound Ero1α had more than 90 % of purity.

To crystallize human Ero1α, a protein surface engineering technique was employed as follows. Lysines on the protein surface were methylated according to the previous

literature (Walter et al., 2006). The methylated sample was further purified by a Superdex 200 column pre-equilibrated with 50 mM Tris-HCl (pH 8.1) and 150 mM NaCl, concentrated to ~ 10 mg/ml, and then dialyzed against water. Methylated Ero1α crystals appeared within a week by vapor diffusion at 20°C. The reservoir conditions were: 8% PEG4000 and 50 mM imidazole (pH 8.0) for the hyperactive form, and 20% PEG1500 and 80 mM imidazole (pH 8.0) for the inactive form. For cryoprotection, the crystals were transferred directly to a 16% glycerol, 100 mM imidazole (pH 8.0) solution containing 20% PEG4000 (for the hyperactive form), or 30% PEG1500 (for the inactive form), and flash-frozen with cold nitrogen gas from a cryostat (Rigaku, Japan).

Crystallographic analysis

Diffraction data were collected at the Osaka University beamline BL44XU at SPring-8 equipped with MX225-HE (Rayonix), which is financially supported by the Academia Sinica and National Synchrotron Radiation Research Center (Taiwan, ROC). Data were integrated with HKL2000 (Otwinowski and Minor, 1997), and the crystallographic parameters are summarized in Table I. Crystals contained one molecule in an asymmetric unit for both hyperactive and inactive Ero1α. Phase determination was made by molecular replacement using the published structure of yeast Ero1p (PDB code 1RP4) as the search model, with the program Molrep (Vagin, 1997). The initial structural model of human Ero1α was constructed using the program ARP/warp (Perrakis et al., 2001), and was refined by several cycles of manual rebuilding and refinement with Coot (Emsley and Cowtan, 2004) and Refmac 5 (Collaborative Computational Project, 1994).

Construction of chimeric proteins between PDI and ERp57

To construct chimeric proteins in which the b'-domain was mutually swapped between PDI and ERp57, *Kpn*I and *Sac*I restriction sites were introduced at the start (234Leu for PDI, 241Phe for ERp57) and end (355Leu for PDI, 365Leu for ERp57) of the b'-domains (Supplemental Fig. 4). The *Kpn*I-*Sac*I fragment of PDI was then inserted into the corresponding sites of the vectors encoding the a-, b-, and a'-domains of ERp57. The PDI-based chimera with the ERp57 b'-domain was similarly prepared. The introduced restriction sites were mutated back to their original sequences using a Quik Mutagenesis Kit with appropriate primer sets. Chimeric proteins, including wild-type PDI and ERp57, were overexpressed in *E. coli* strain BL21(DE3). LB medium containing 50 μg ml^{-1} ampicillin was grown at 37°C until IPTG was added to the medium at a final concentration of 0.5 mM at A_{600} = ~ 0.5. After an additional 4 h of shaking at 30°C, cells were harvested. The cell lysate supernatant was applied to the Ni-NTA Sepharose open column. Fractions eluted with 200 mM imidazole were further purified by anion exchange chromatography with a MonoQ column. Each construct was quantified using the BCA method.

Oxygen consumption assay

Oxygen consumption was measured using a Clark-type oxygen electrode (YSI 5331). All experiments were performed at 30°C in air-saturated buffer (~235 μM O_2) in 50 mM Tris-HCl (pH 8.1), 150 mM NaCl. Catalytic oxygen consumption was initiated by adding each Ero1α variant to a final concentration of 2 μM in a reaction mixture containing 10 μM PDI or its derivatives and 10 mM GSH.

Surface plasmon resonance (SPR) measurements

The association and dissociation rate constants (k_{on} or k_{off}) for the direct binding of PDI, ERp57, or their chimeric proteins to immobilized Ero1α were determined by SPR measurements on a BIACORE2000 system (GE Healthcare). The hyperactive or inactive form of Ero1α was coupled to the CM5 sensor chip (GE Healthcare) using amine-coupling chemistry. As a control, one channel was coupled with bovine serum albumin (BSA) to exclude background binding. Before monitoring analyte binding, immobilized Ero1α was activated with 2 μM reduced PDI dissolved in a buffer containing 10 mM GSH. Sensorgrams were recorded for three concentrations of each analyte sample (2, 4, and 8 μM for PDI and ERp57-based chimera; and 8, 16, and 32 μM for ERp57 and PDI-based chimera) at 25°C for a 2 min association phase, followed by a 4 min dissociation phase. The running buffer was 20 mM HEPES-NaOH (pH 7.4), 150 mM NaCl, 0.001% Tween-20, 2 mM EDTA, 1 mM GSH, and 0.25 mM GSSG. All analyte samples were exchanged and diluted into this buffer beforehand. We verified by oxygen consumption assay that the presence of 0.001% Tween-20 only modestly inhibited Ero1α-catalysed PDI oxidation (Supplemental Fig. S11). Sensorgrams were analyzed by nonlinear regression analysis according to a two-state model using the BIAevaluation 4.1 software. Experiments were replicated at least four times.

Acknowledgements

We thank Kazutaka Araki and Kazuhiro Nagata for stimulating discussion and helpful advice on the oxygen consumption and SPR measurements; Eiki Yamashita and Atsushi

Nakagawa for help with diffraction data collection; and Claudio Fagioli and Akiko Sato for technical support. We also thank Tomohisa Horibe and Masakazu Kikuchi for kindly providing the ERp57 expression vector. This work was supported by a Grant-in-Aid for Young Scientists (A) from MEXT and the Yamada Science Foundation (to K. Inaba), AIRC, Fondazione Cariplo and Telethon (to R.Sitia) and by the Targeted Proteins Research Program (TPRP) from MEXT (to M. Suzuki). Regarding author contributions, K. Inaba carried out most of the crystallographic works and a portion of the functional analyses. S. Masui and H. Iida performed most of the functional analyses. S. Vavassori and R. Sitia greatly contributed to editing the manuscript. M. Suzuki carried out diffraction data analysis and structure refinement. All authors discussed the results and commented on the manuscript. K. Inaba supervised the work and wrote the manuscript.

Accession Numbers

The coordinates and structural factors described in this study have been deposited in the Protein Data Bank with ID code 3AHQ for the hyperactive form of human Ero1α and 3AHR for the inactive form of human Ero1α.

References

Appenzeller-Herzog, C., and Ellgaard, L. (2008). The human PDI family: versatility packed into a single fold. Biochimica et Biophysica Acta *1783*, 535-548.

Appenzeller-Herzog, C., Riemer, J., Christensen, B., Sorensen, E.S., and Ellgaard, L. (2008). A novel disulphide switch mechanism in Ero1alpha balances ER oxidation in human cells. EMBO Journal *27*, 2977-2987.

Baker, K.M., Chakravarthi, S., Langton, K.P., Sheppard, A.M., Lu, H., and Bulleid, N.J. (2008). Low reduction potential of Ero1alpha regulatory disulphides ensures tight control of substrate oxidation. EMBO Journal *27*, 2988-2997.

Benham, A.M., Cabibbo, A., Fassio, A., Bulleid, N., Sitia, R., and Braakman, I. (2000). The CXXCXXC motif determines the folding, structure and stability of human Ero1-Lalpha. EMBO Journal *19*, 4493-4502.

Bertoli, G., Simmen, T., Anelli, T., Molteni, S.N., Fesce, R., and Sitia, R. (2004). Two conserved cysteine triads in human Ero1alpha cooperate for efficient disulfide bond formation in the endoplasmic reticulum. Journal of Biological Chemistry *279*, 30047-30052.

Cabibbo, A., Pagani, M., Fabbri, M., Rocchi, M., Farmery, M.R., Bulleid, N.J., and Sitia, R. (2000). ERO1-L, a human protein that favors disulfide bond formation in the endoplasmic reticulum. Journal of Biological Chemistry *275*, 4827-4833.

Collaborative Computational Project, N. (1994). The CCP4 suite: programs for protein crystallogaaphy. Acta Crystallographica Section D-Biological Crystallography *50*, 760-763.

Denisov, A.Y., Maattanen, P., Dabrowski, C., Kozlov, G., Thomas, D.Y., and Gehring, K. (2009). Solution structure of the bb' domains of human protein disulfide isomerase. FEBS Journal *276*, 1440-1449.

Dias-Gunasekara, S., Gubbens, J., van Lith, M., Dunne, C., Williams, J.A., Kataky, R., Scoones, D., Lapthorn, A., Bulleid, N.J., and Benham, A.M. (2005). Tissue-specific expression and dimerization of the endoplasmic reticulum oxidoreductase Ero1beta. Journal of Biological Chemistry *280*, 33066-33075.

Dong, G., Wearsch, P.A., Peaper, D.R., Cresswell, P., and Reinisch, K.M. (2009). Insights into MHC class I peptide loading from the structure of the tapasin-ERp57 thiol oxidoreductase heterodimer. Immunity *30*, 21-32.

Dym, O., and Eisenberg, D. (2001). Sequence-structure analysis of FAD-containing proteins. Protein Science *10*, 1712-1728.

Ellgaard, L., Molinari, M., and Helenius, A. (1999). Setting the standards: quality control in the secretory pathway. Science *286*, 1882-1888.

Ellgaard, L., and Ruddock, L.W. (2005). The human protein disulphide isomerase family: substrate interactions and functional properties. EMBO Reports *6*, 28-32.

Emsley, P., and Cowtan, K. (2004). Coot: model-building tools for molecular graphics. Acta Crystallographica Section D-Biological Crystallography *60*, 2126-2132.

Fass, D. (2008). The Erv family of sulfhydryl oxidases. Biochimica et Biophysica Acta *1783*, 557-566.

Frand, A.R., and Kaiser, C.A. (1998). The ERO1 gene of yeast is required for oxidation

of protein dithiols in the endoplasmic reticulum. Molecular Cell *1*, 161-170.

Gross, E., Kastner, D.B., Kaiser, C.A., and Fass, D. (2004). Structure of Ero1p, source of disulfide bonds for oxidative protein folding in the cell. Cell *117*, 601-610.

Gross, E., Sevier, C.S., Heldman, N., Vitu, E., Bentzur, M., Kaiser, C.A., Thorpe, C., and Fass, D. (2006). Generating disulfides enzymatically: reaction products and electron acceptors of the endoplasmic reticulum thiol oxidase Ero1p. Proceedings of the National Academy of Sciences of the United States of America *103*, 299-304.

Harding, H.P., Zhang, Y., Zeng, H., Novoa, I., Lu, P.D., Calfon, M., Sadri, N., Yun, C., Popko, B., Paules, R., *et al.* (2003). An integrated stress response regulates amino acid metabolism and resistance to oxidative stress. Molecular Cell *11*, 619-633.

Hatahet, F., Ruddock, L.W., Ahn, K., Benham, A., Craik, D., Ellgaard, L., Ferrari, D., and Ventura, S. (2009). Protein disulfide isomerase: a critical evaluation of its function in disulfide bond formation. Antioxidants & Redox Signaling *11*, 2807-2850.

Haynes, C.M., Titus, E.A., and Cooper, A.A. (2004). Degradation of misfolded proteins prevents ER-derived oxidative stress and cell death. Molecular Cell *15*, 767-776.

Heckler, E.J., Rancy, P.C., Kodali, V.K., and Thorpe, C. (2008). Generating disulfides with the Quiescin-sulfhydryl oxidases. Biochimica et Biophysica Acta *1783*, 567-577.

Inaba, K., and Ito, K. (2008). Structure and mechanisms of the DsbB-DsbA disulfide bond generation machine. Biochimica et Biophysica Acta *1783*, 520-529.

Jansens, A., van Duijn, E., and Braakman, I. (2002). Coordinated nonvectorial folding in a newly synthesized multidomain protein. Science *298*, 2401-2403.

Jessop, C.E., Chakravarthi, S., Garbi, N., Hammerling, G.J., Lovell, S., and Bulleid, N.J. (2007). ERp57 is essential for efficient folding of glycoproteins sharing common structural domains. EMBO Journal *26*, 28-40.

Karala, A.R., Lappi, A.K., Saaranen, M.J., and Ruddock, L.W. (2009). Efficient peroxide-mediated oxidative refolding of a protein at physiological pH and implications for oxidative folding in the endoplasmic reticulum. Antioxidants & Redox Signaling *11*, 963-970.

Klappa, P., Ruddock, L.W., Darby, N.J., and Freedman, R.B. (1998). The b' domain provides the principal peptide-binding site of protein disulfide isomerase but all domains contribute to binding of misfolded proteins. EMBO Journal *17*, 927-935.

Kozlov, G., Maattanen, P., Schrag, J.D., Pollock, S., Cygler, M., Nagar, B., Thomas, D.Y., and Gehring, K. (2006). Crystal structure of the bb' domains of the protein disulfide isomerase ERp57. Structure *14*, 1331-1339.

Marciniak, S.J., Yun, C.Y., Oyadomari, S., Novoa, I., Zhang, Y., Jungreis, R., Nagata, K., Harding, H.P., and Ron, D. (2004). CHOP induces death by promoting protein synthesis and oxidation in the stressed endoplasmic reticulum. Genes & Development *18*, 3066-3077.

Mezghrani, A., Fassio, A., Benham, A., Simmen, T., Braakman, I., and Sitia, R. (2001). Manipulation of oxidative protein folding and PDI redox state in mammalian cells. EMBO Journal *20*, 6288-6296.

Nguyen, V.D., Wallis, K., Howard, M.J., Haapalainen, A.M., Salo, K.E., Saaranen, M.J., Sidhu, A., Wierenga, R.K., Freedman, R.B., Ruddock, L.W., and Williamson, R.A. (2008). Alternative conformations of the x region of human protein disulphide-isomerase modulate exposure of the substrate binding b' domain. Journal of Molecular Biology *383*, 1144-1155.

Oliver, J.D., Roderick, H.L., Llewllyn, D.H., and High, S. (1999). ERp57 functions as a subunit of specific complexes formed with the ER lectins calreticulin and calnexin. Mol. Biol. Cell *10*, 2573-2582.

Oliver, J.D., van der Wal, F. J., Bulleid, N. J. and High, S. (1997). Interaction of the thiol-dependent reductase ERp57 with nascent glycoproteins. Science *275*, 86-88.

Otsu, M., Bertoli, G., Fagioli, C., Guerini-Rocco, E., Nerini-Molteni, S., Ruffato, E., and Sitia, R. (2006). Dynamic retention of Ero1alpha and Ero1beta in the endoplasmic reticulum by interactions with PDI and ERp44. Antioxidants & Redox Signaling *8*, 274-282.

Otwinowski, Z., and Minor, W. (1997). Processing of X-ray Diffraction Data Collected in Oscillation Mode. Methods in Enzymology *276*, 307-326.

Pagani, M., Fabbri, M., Benedetti, C., Fassio, A., Pilati, S., Bulleid, N.J., Cabibbo, A., and Sitia, R. (2000). Endoplasmic reticulum oxidoreductin 1-lbeta (ERO1-Lbeta), a human gene induced in the course of the unfolded protein response. Journal of Biological Chemistry *275*, 23685-23692.

Perrakis, A., Harkiolaki, M., Wilson, K.S., and Lamzin, V.S. (2001). ARP/wARP and molecular replacement. Acta Crystallographica Section D-Biological Crystallography *57*, 1445-1450.

Pollard, M.G., Travers, K.J., and Weissman, J.S. (1998). Ero1p: a novel and ubiquitous protein with an essential role in oxidative protein folding in the endoplasmic reticulum. Molecular Cell *1*, 171-182.

Russell, S.J., Ruddock, L.W., Salo, K.E., Oliver, J.D., Roebuck, Q.P., Llewellyn, D.H., Roderick, H.L., Koivunen, P., Myllyharju, J., and High, S. (2004). The primary substrate

binding site in the b' domain of ERp57 is adapted for endoplasmic reticulum lectin association. Journal of Biological Chemistry *279*, 18861-18869.

Serve, O., Kamiya, Y., Maeno, A., Nakano, M., Murakami, C., Sasakawa, H., Yamaguchi, Y., Harada, T., Kurimoto, E., Yagi-Utsumi, M.*, et al.* (2010). Redox-dependent domain rearrangement of protein disulfide isomerase coupled with exposure of its substrate-binding hydrophobic surface. Journal of Molecular Biology *396*, 361-374.

Sevier, C.S., Cuozzo, J.W., Vala, A., Aslund, F., and Kaiser, C.A. (2001). A flavoprotein oxidase defines a new endoplasmic reticulum pathway for biosynthetic disulphide bond formation. Nature Cell Biology *3*, 874-882.

Sevier, C.S., Kadokura, H., Tam, V.C., Beckwith, J., Fass, D., and Kaiser, C.A. (2005). The prokaryotic enzyme DsbB may share key structural features with eukaryotic disulfide bond forming oxidoreductases. Protein Science *14*, 1630-1642.

Sevier, C.S., and Kaiser, C.A. (2006). Conservation and diversity of the cellular disulfide bond formation pathways. Antioxidants & Redox Signaling *8*, 797-811.

Sevier, C.S., and Kaiser, C.A. (2008). Ero1 and redox homeostasis in the endoplasmic reticulum. Biochimica et Biophysica Acta *1783*, 549-556.

Sevier, C.S., Qu, H., Heldman, N., Gross, E., Fass, D., and Kaiser, C.A. (2007). Modulation of cellular disulfide-bond formation and the ER redox environment by feedback regulation of Ero1. Cell *129*, 333-344.

Streyer, L. (1965). The inetraction of a naphthalene dye with apomyoglobin and apohemoglobin. A fluorecent probe of non-polar binding sites. Journal of Molecular Biology *13*, 482-495.

Tavender, T.J., and Bulleid, N.J. (2010). Molecular mechanisms regulating oxidative activity of the Ero1 family in the endoplasmic reticulum. Antioxidant & Redox Signaling *in press*.

Tian, G., Kober, F.X., Lewandrowski, U., Sickmann, A., Lennarz, W.J., and Schindelin, H. (2008). The catalytic activity of protein-disulfide isomerase requires a conformationally flexible molecule. Journal of Biological Chemistry *283*, 33630-33640.

Tian, G., Xiang, S., Noiva, R., Lennarz, W.J., and Schindelin, H. (2006). The crystal structure of yeast protein disulfide isomerase suggests cooperativity between its active sites.[erratum appears in Cell. 2006 Mar 10;124(5):1085-8]. Cell *124*, 61-73.

Tu, B.P., and Weissman, J.S. (2004). Oxidative protein folding in eukaryotes: mechanisms and consequences. Journal of Cell Biology *164*, 341-346.

Vagin, A.a.T., A., (1997). MOLREP: an automated program for molecular replacement.

Jounal of Applied Crystallogarphy *30*, 1022-1025.

Veal, E.A., Day, A.M., and Morgan, B.A. (2007). Hydrogen peroxide sensing and signaling. Molecular Cell *26*, 1-14.

Vitu, E., Kim, S., Sevier, C.S., Lutzky, O., Heldman, N., Bentzur, M., Unger, T., Yonda, M., Kaiser, C.A., and Fass, D. (2010). Oxidative activity of yeast Ero1p on protein disulfide isomerase and related oxidoreductases of the endoplasmic reticulum. Journal of Biological Chemistry *285*, 18155-18165.

Walter, T.S., Meier, C., Assenberg, R., Au, K.F., Ren, J., Verma, A., Nettleship, J.E., Owens, R.J., Stuart, D.I., and Grimes, J.M. (2006). Lysine methylation as a routine rescue strategy for protein crystallization. Structure *14*, 1617-1622.

Wang C, C., S, Wang, X, Wang, L, Wallis, AK, Freedman, RB, Wang, CC (2010). Plasticity of human protein disulfide isomerase: evidence for mobility around the x-linker region and its functional significance. J. Biol. Chem. *in press*.

Wang, L., Li, S.J., Sidhu, A., Zhu, L., Liang, Y., Freedman, R.B., and Wang, C.C. (2009). Reconstitution of human Ero1-Lalpha/protein-disulfide isomerase oxidative folding pathway in vitro. Position-dependent differences in role between the a and a' domains of protein-disulfide isomerase. Journal of Biological Chemistry *284*, 199-206.

Zito, E., Chin, K.-T., Blais, H., and Ron, D. (2010). Ero1-beta, a pancreas-specific disulfide oxidase, pomotes insulin biogenesis and glucose homeostasis. Journal of Cell Biology *188*, 821-832.

Figure Legends

Fig. 1. Amino acid sequence, secondary structure, and disulphide connectivity of human Ero1α and yeast Ero1p.

(A) Sequence alignment of human Ero1α and yeast Ero1p using Clustal W. Cylinders and arrows above the sequences represent determined α-helices and β-strands in human Ero1α, respectively. Helices constituting the four-helix bundle in the catalytic core region are shown by dark blue cylinders. Gray amino acids denote loop regions with invisible electron density. Regulatory cysteines and active-site cysteines are shown in red and green, respectively. Dotted lines connecting yellow circles indicate the characterized structural disulphides in human Ero1α. The broken line at the N-terminal region indicates the signal sequence.

(B) Hyperactive and inactive mutants of human and yeast Ero1s. While cysteine residues are shown with yellow circles, the Cys to Ala mutation sites in the Ero1 mutants are represented by gray circles. Structural, regulatory, and active-site disulphides, which are based on the previous studies (Appenzeller-Herzog et al., 2008; Baker et al., 2008; Sevier et al., 2007), are represented by black, red and green lines, respectively. In yeast Ero1p, Cys90-Cys349 also seems to function as a regulatory disulphide since the reduction of Cys90-Cys349 as well as Cys150-Cys295 was observed during the Ero1p catalysis (Sevier et al., 2007).

(C) Oxygen consumption by wild-type Ero1α and its hyperactive and inactive mutants constructed in this work during the oxidation of human PDI in the presence of 10 mM reduced glutathione (GSH). A control reaction following oxygen consumption in the absence of Ero1α (GSH/PDI only) is as indicated.

Fig. 2 Overall structure of human Ero1α

(A) Ribbon diagram of the hyperactive form of human Ero1α. Loop segments that could not be modeled due to the lack of electron density are shown by dotted lines. The regulatory loop including Cys94, Cys99, Cys104, and Cys131 is illustrated by a red dotted line. Structural and active-site disulphides characterized in this study are represented by sticks. The four-helix bundle constituting the catalytic core region of Ero1α is in dark blue. The FAD molecule is represented by balls, in which carbon, nitrogen, oxygen, and phosphorus atoms are in yellow, blue, red, and orange, respectively.

(B) Close-up view of the N-terminal region of human Ero1α. Disulphide bridges formed in this region are represented by sticks. Numbers indicate the residue number from the N-terminus.

(C) Superimposition of human Ero1α and yeast Ero1p. Crystal structures of the hyperactive form of human Ero1α (magenta) and yeast Ero1p (green) are superimposed such that the RMSD between their C_α atoms is minimized. Dotted square represents the four-helix bundle scaffold shared by the two Ero1s. Inset highlights the structural differences between the Ero1s, and is viewed from a different angle to clearly show the regulatory disulphide between Cys150 and Cys295 in yeast Ero1p.

Fig. 3 FAD-binding site in human Ero1α

(A) FAD and its neighboring structure in human Ero1α. The FAD moiety and side

chains of Tyr191, Cys394, and Cys397 are represented by sticks.

(B) FAD-binding mode in human Ero1α (magenta) and yeast Ero1p (green). Residues involved in aromatic ring stacking and van der Waals contact with the FAD moiety are numbered (red for human Ero1α, green for yeast Ero1p) and shown in stick representation.

(C) Proposed chemical scheme of *de novo* disulphide bond generation by the cooperation of the Cys394-Cys397 pair of human Ero1α and FAD.

(D) Accommodation of the isoalloxazine ring inside the four-helix bundle scaffold. The four-helix bundle and loop segment (residues 183-194) just above the isoalloxazine ring are shown in dark blue and light green, respectively. The β-hairpin region (residues 265-279) is removed for a clear view of the region.

Fig. 4 Structural basis of Ero1α regulation

(A) Local conformational changes upon disulphide rearrangement within the regulatory loop region. The Cys94-Cys131 disulphide formed in inactive Ero1α is shown in stick representation. The electron density map is shown at the 1.0 contour level.

(B) Geometry of the Cys94-Cys131 inhibitory disulphide relative to the Cys394-Cys397 active-site disulphide. The FAD moiety and side chains of Cys94, Cys131, Cys394, and Cys397 are represented by sticks. The loop region (residues 188-193) is removed for a clear view of the region.

(C) Affinity measurements between human PDI and Ero1α variants by surface plasmon resonance spectroscopy. Hyperactive (left) or inactive (right) Ero1α variant was immobilized on a biosensor chip, and PDI at 2 μM (green), 4 μM (blue), or 8 μM

(red) was injected as analyte in the presence of 1 mM GSH and 0.25 mM GSSG. Calculated kinetic parameters for binding of human PDI to hyperactive or inactive Ero1α are compiled in the lower panel.

Fig. 5 Increased mobility of the regulatory loop restores activity of inactive Ero1α.

(A) Schematic representation of glycine-repeat insertion into the site after Cys131.

(B) Oxygen consumption by inactive Ero1α variants with different lengths of glycine-repeat insertions during human PDI oxidation in the presence of 10 mM GSH. A control reaction following oxygen consumption in the absence of Ero1α (GSH/PDI only) is as indicated.

Fig. 6 Critical role of the PDI b'-domain in the specific PDI oxidation by Ero1α

(A) Chimeric proteins between human PDI and ERp57 constructed in this study. Domains deriving from PDI and ERp57 are shown in pink and blue, respectively. The domain boundaries of the constructs are described in Materials and methods.

(B) Oxygen consumption by the hyperactive Ero1α variant during oxidation of human PDI, ERp57, and the two chimeric proteins in the presence of 10 mM GSH.

(C) Measurements of the affinity for hyperactive Ero1α with PDI, ERp57, and the two chimeric proteins by surface plasmon resonance. The Ero1α mutant was immobilized on a biosensor chip. For PDI and ERp57-based chimera, 2 μM (green), 4 μM (blue), or 8 μM (red) samples were injected in the presence of 1 mM GSH and 0.25 mM GSSG as analytes. For ERp57 and PDI-based chimera, 8 μM (red), 16 μM (orange) or 32 μM (purple) samples were injected similarly. Association and dissociation rate

constants were determined using a two-state reaction model, and the kinetic parameters are summarized in the bottom panel. Data represent the means from at least four individual experiments.

Fig. 7 Electrostatic and hydrophobic interactions mediate specificity of the Ero1α-PDI interplay

(A) Electrostatic surface representation of human Ero1α. The orientation of human Ero1α is the same as in Fig. 2A. The regulatory loop and the nearby positively charged patch in Ero1α are indicated by a dotted line and an oval, respectively. Regions of basic potential are blue (> 20 k_BT/e) and acidic regions are red (< -20 k_BT/e).

(B) Positively charged residues near the regulatory loop are highlighted. The side chains of Arg83, Arg383 and Arg387 are represented by sticks.

(C) Oxygen consumption by the RD, RA and hyperactive mutants of Ero1α during oxidation of human PDI in the presence of 10 mM GSH. NaCl concentration was fixed at 0.3 M.

(D) Oxygen consumption by the hyperactive Ero1α variant during oxidation of human PDI in the presence of 10 mM GSH and various concentrations of NaCl.

(E-H) As in (D). Various concentrations of Triton X-100 (E), ANS (F), somatostatin (G) or mastoparan (H) were added to the reaction buffer, while NaCl concentration was fixed at 0.3 M.

Table I *Data collection and structure determination*

	human Ero1α Cys104&131Ala (hyperactive)	human Ero1α Cys99&104Ala (inactive)
Data collection		
Beamline	BL44XU at SPring-8	BL44XU at SPring-8
Space group	*I222*	*I222*
Cell dimensions (Å)	*a* = 55.0, *b* = 140.7, *c* = 144.9	*a* = 54.7, *b* = 139.1, *c* = 143.5
	α = β= γ = 90.0°	α = β= γ = 90.0°
Wavelength (Å)	0.90000	0.90000
Resolution range (Å)	41.50-2.35 (2.47-2.35)	36.01-3.07 (3.24-3.07)
No. of total observations	174,207 (24,584)	37,535 (5,172)
No. of unique reflections	23,814 (3,458)	10,434 (1,419)
Completeness (%)	99.3 (99.8)	98.7 (93.1)
$I / \sigma(I)$	21.0 (4.4)	13.8 (2.9)
Multiplicity	7.3 (7.1)	3.6 (3.6)
R_{merge} [a]	0.054 (0.439)	0.063 (0.428)
Refinement		
Resolution range (Å)	36.27-2.35	36.01-3.07
R_{work} [b]	0.237	0.224
R_{free} [c]	0.282	0.303
RMS deviation		
Bond length (Å)	0.018	0.015
Bond angle (°)	1.7	1.6
Ramachandran analysis[e]		
Most favored (%)	89.7	85.5
Allowed (%)	10.0	13.5
Generously allowed (%)	0.3	0.9
Disallowed (%)	0.0	0.0

The number in parentheses represent statistics in the highest resolution shell.
[a] $R_{merge} = \Sigma\Sigma_j|<I(h)> - I(h)_j| / \Sigma\Sigma_j|<I(h)>|$, where $<I(h)>$ is the mean intensity of symmetry-equivalent reflections. [b] $R_{work} = \Sigma(||F_p(obs)| - |F_p(calc)||)/\Sigma|F_p(obs)|$. [c] R_{free} = *R* factor for a selected subset (5 %) of the reflections that was not included in prior refinement calculations.

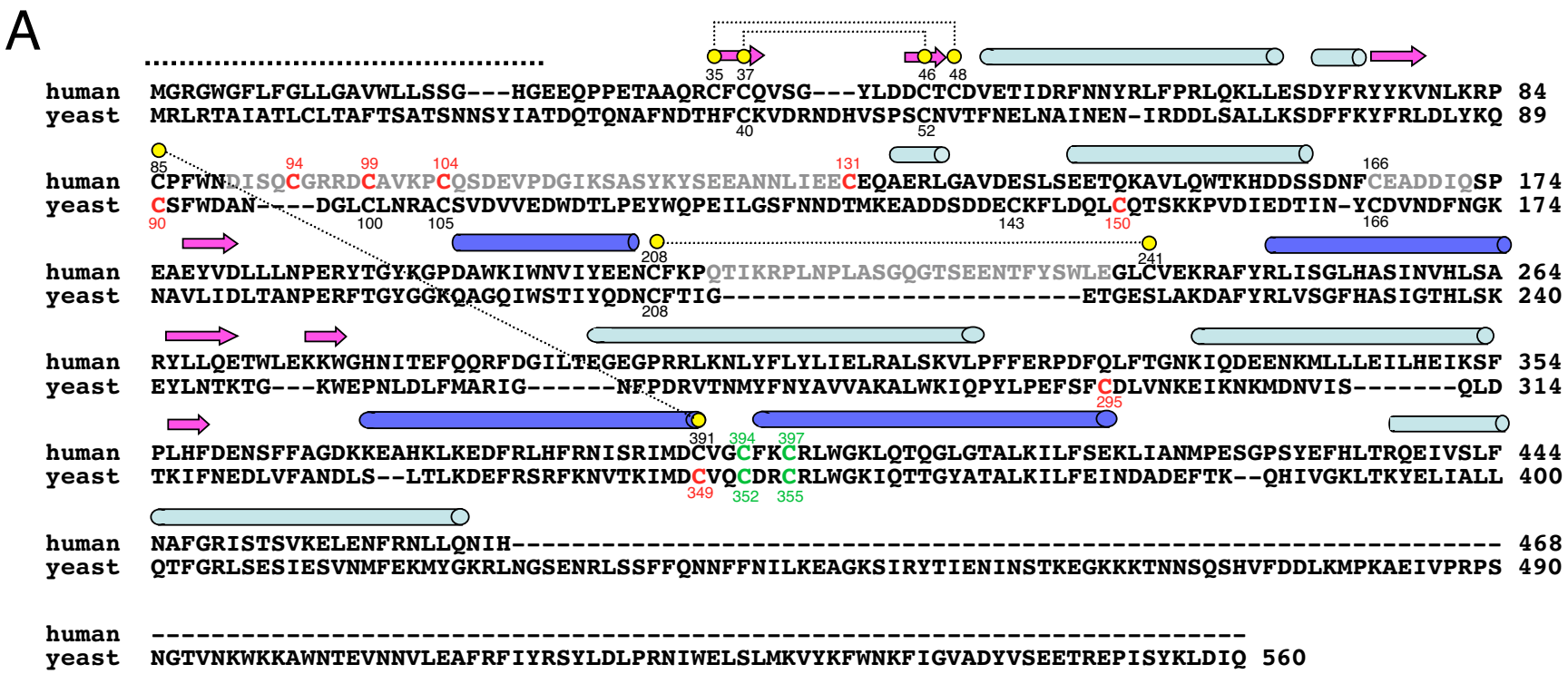

Fig. 1 Inaba et al.

A

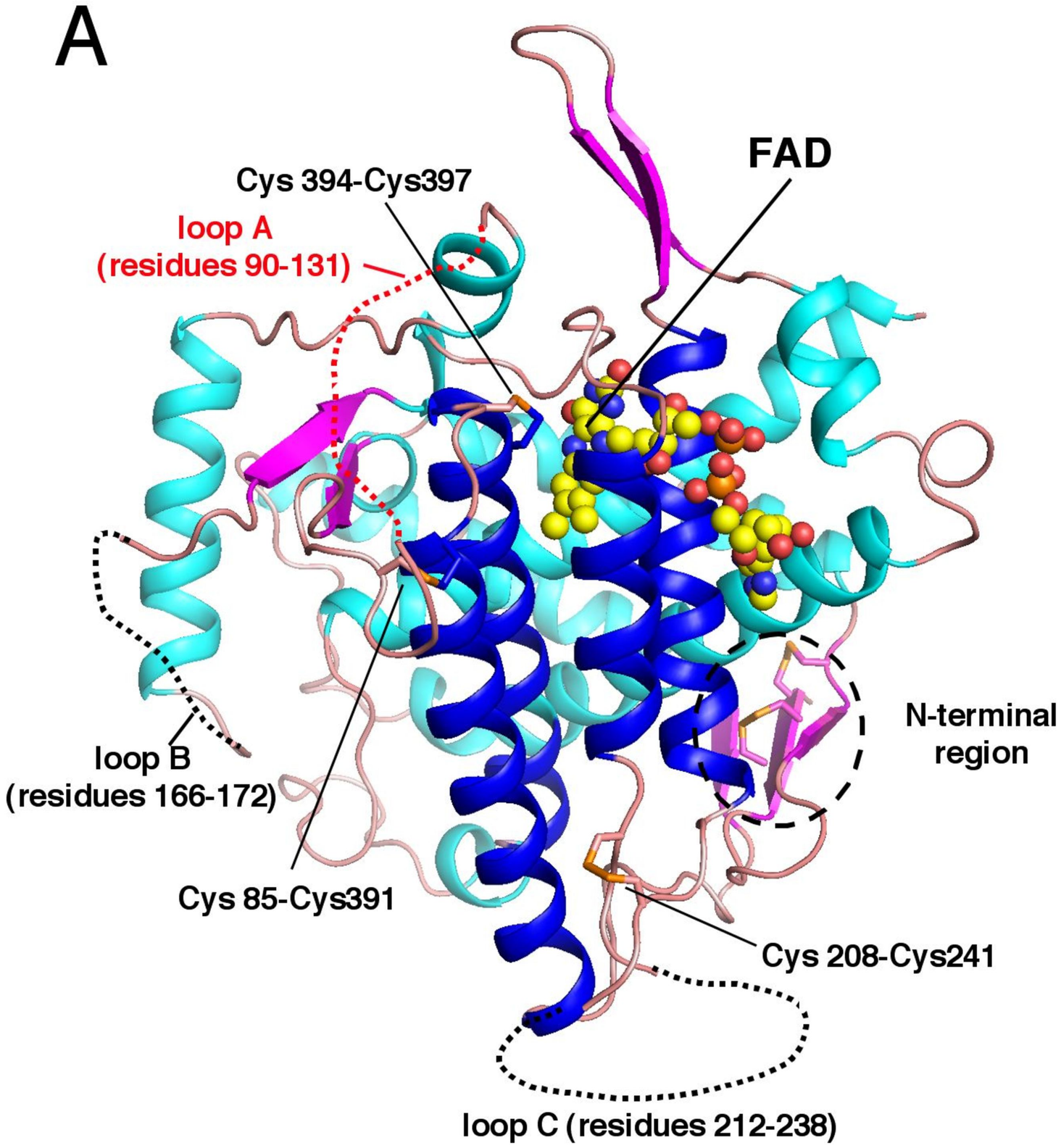

B

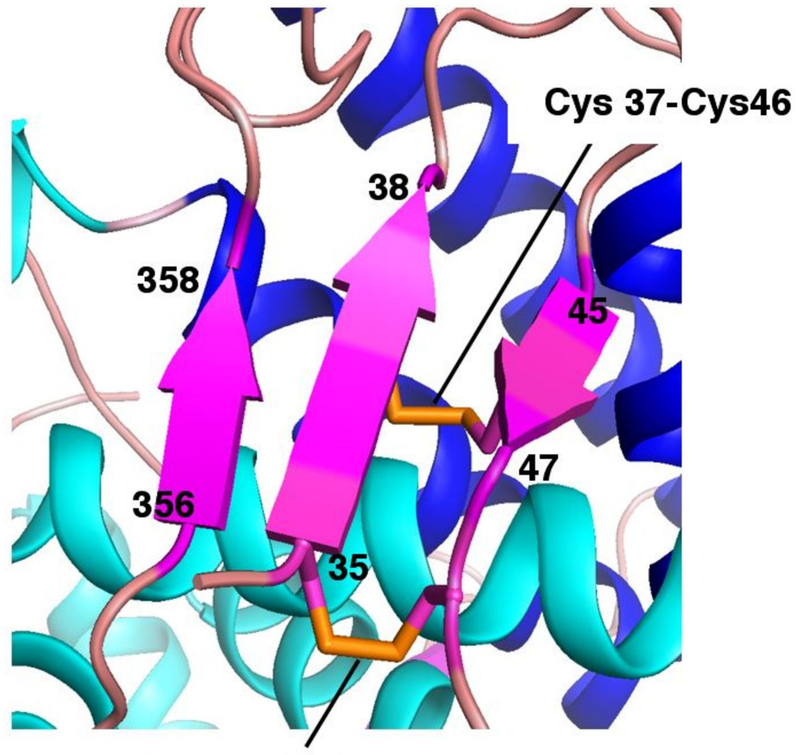

C

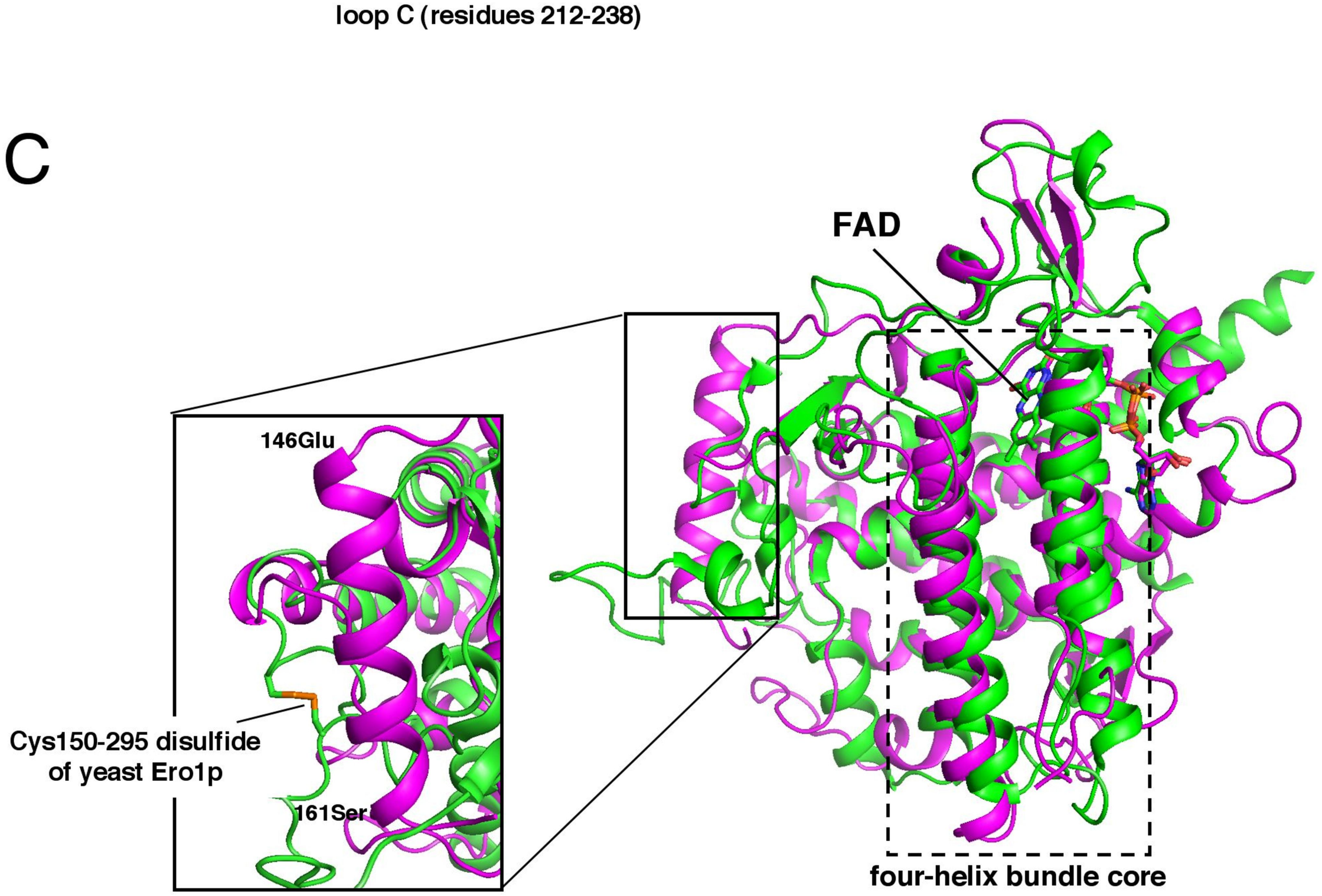

Fig. 2 Inaba et al.

A

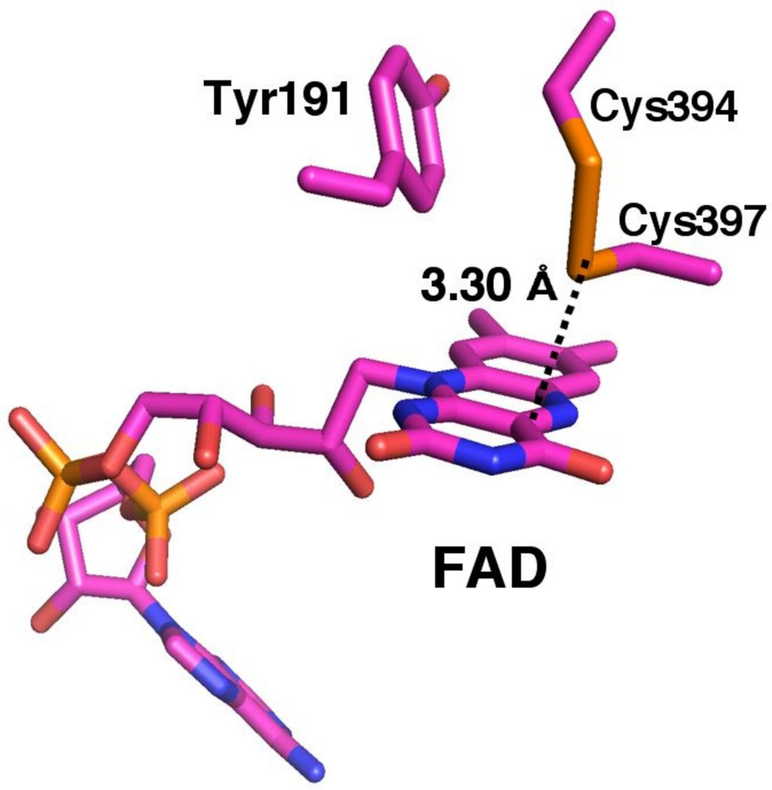

B

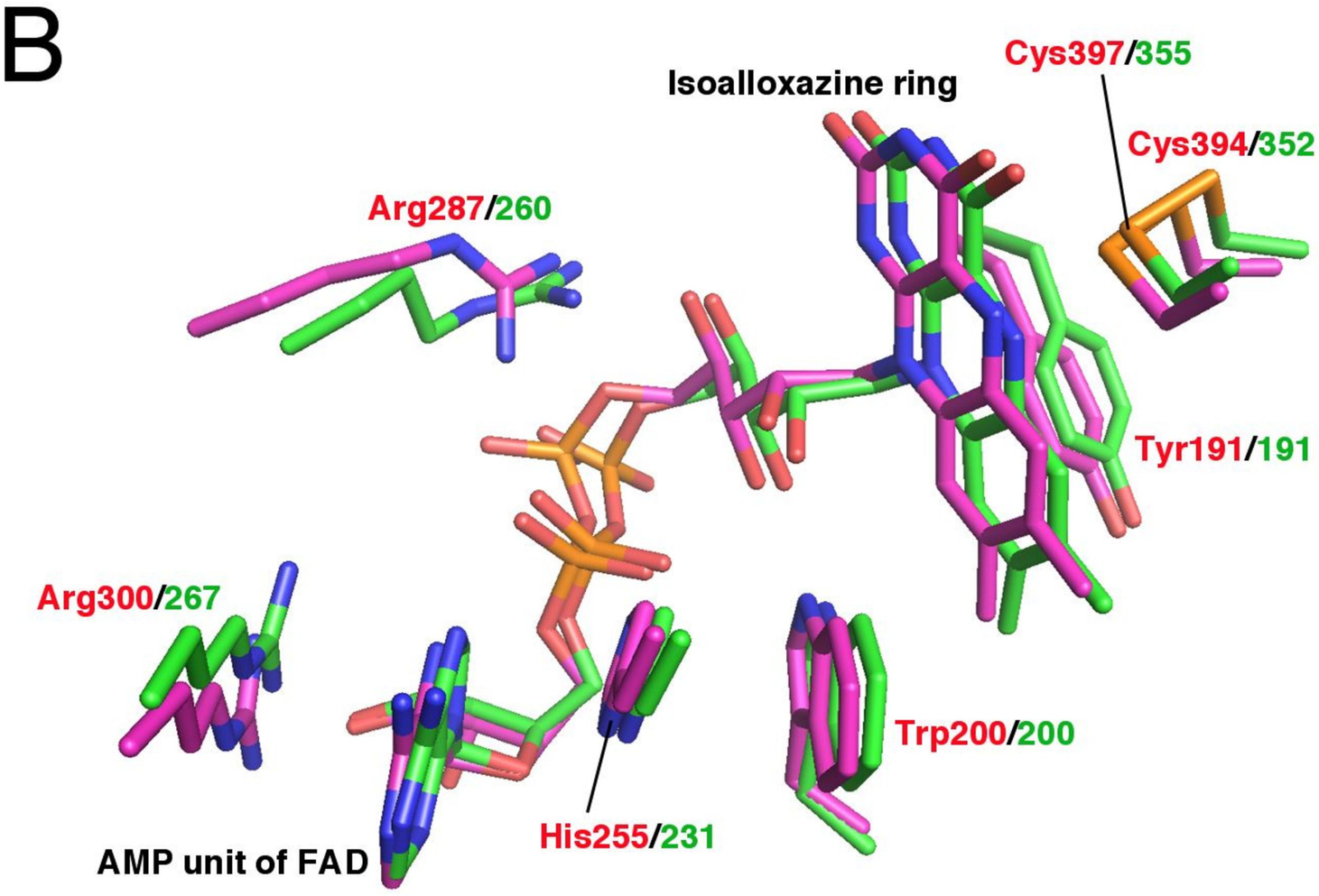

C

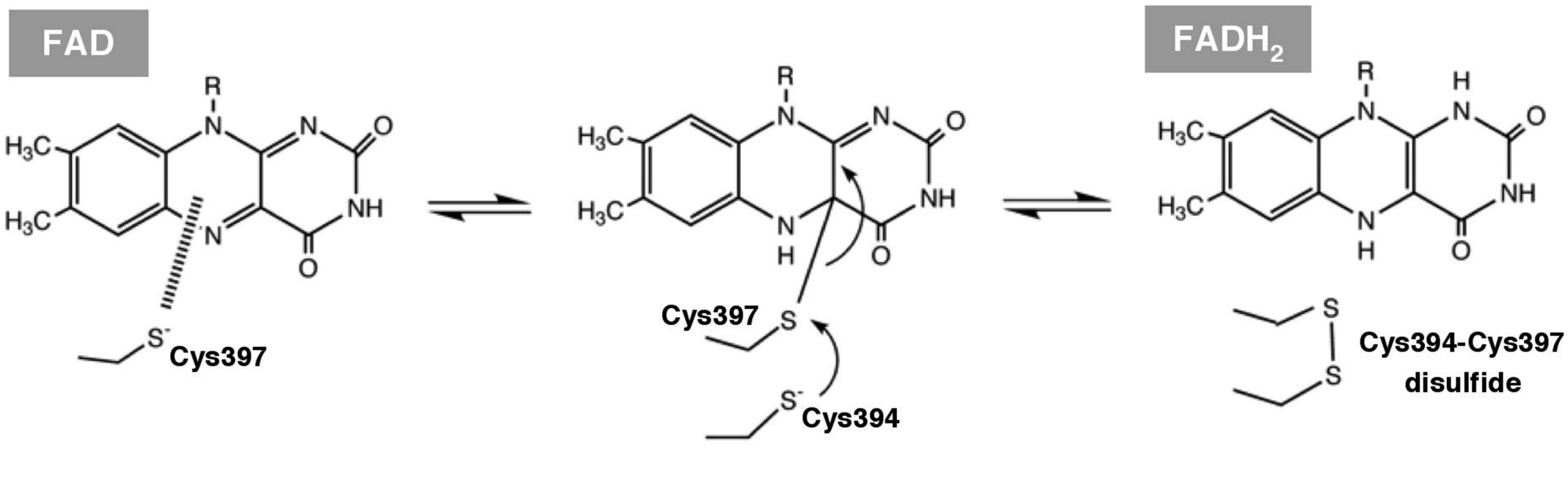

D

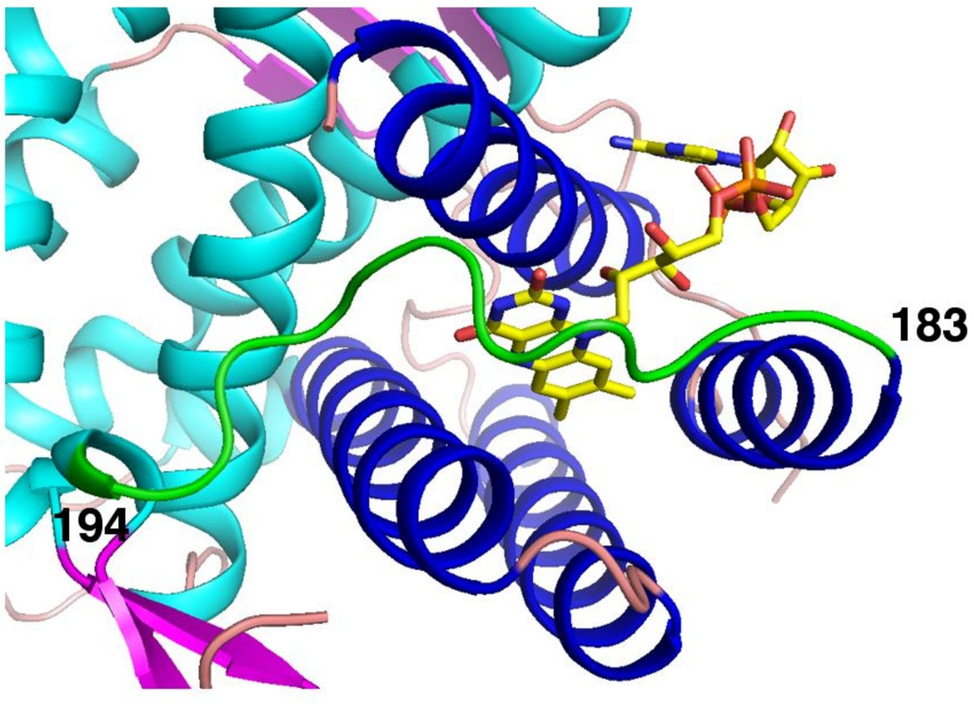

Fig. 3 Inaba et al.

A

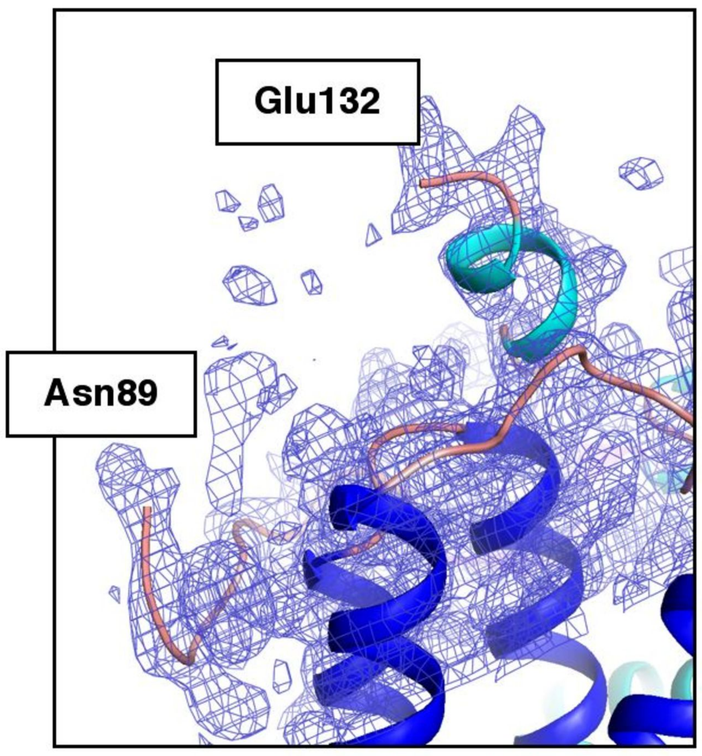

hyperactive form
(Cys94-Cys99)

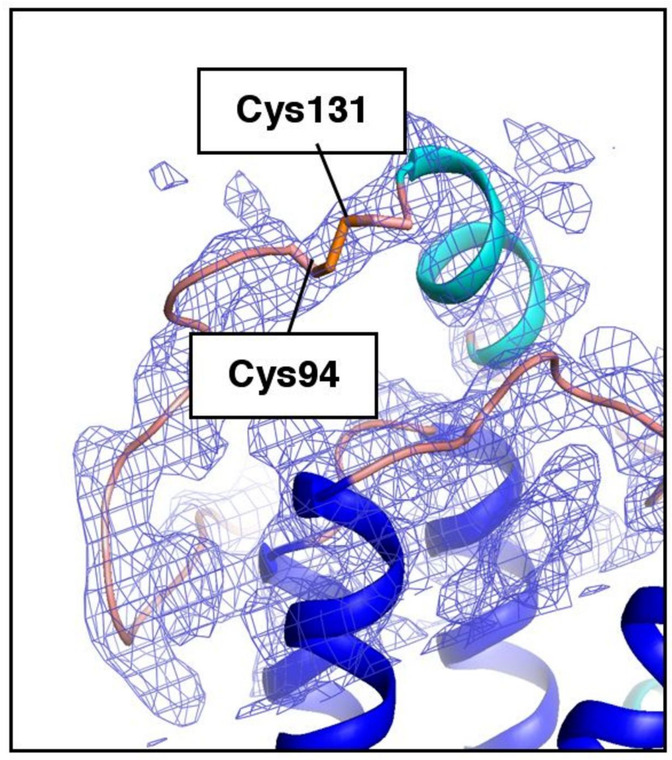

inactive form
(Cys94-Cys131)

B

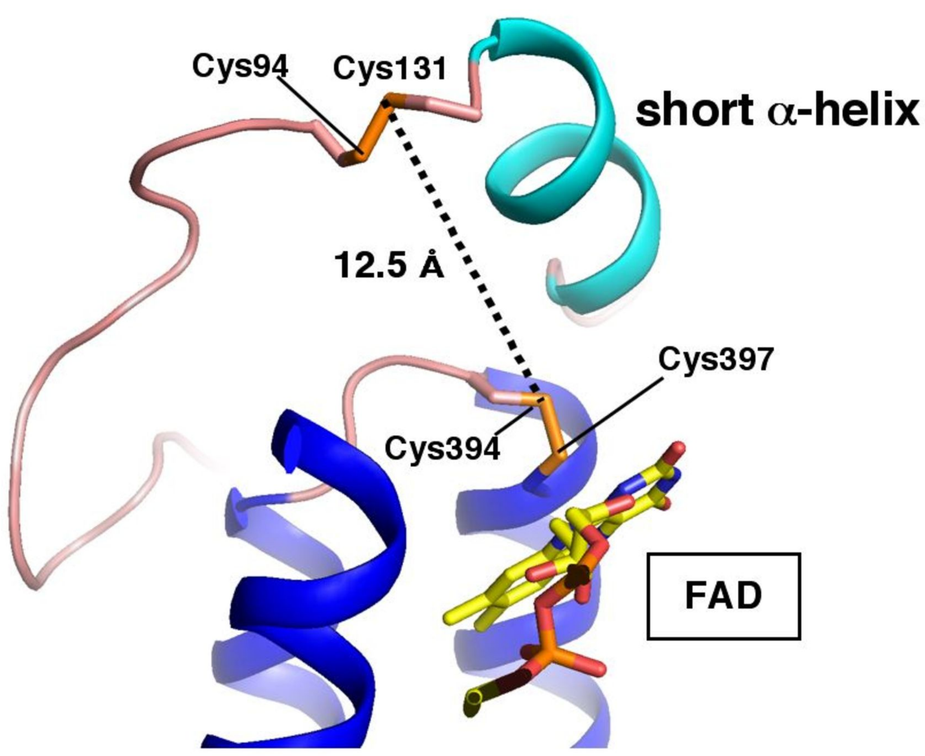

C

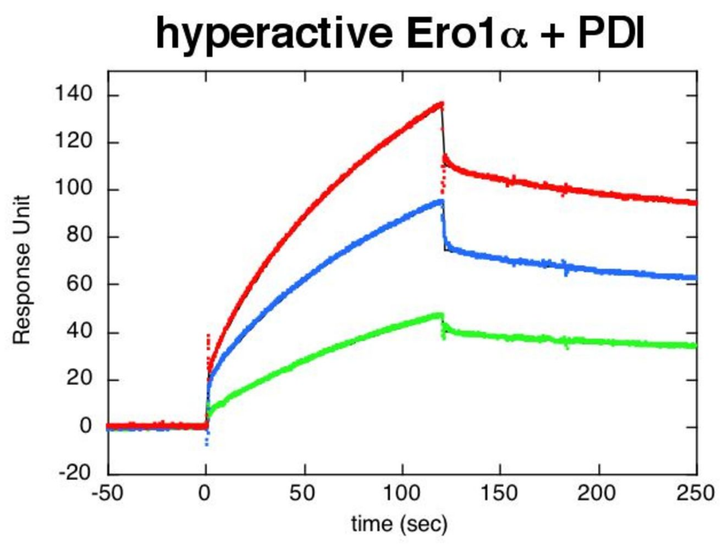

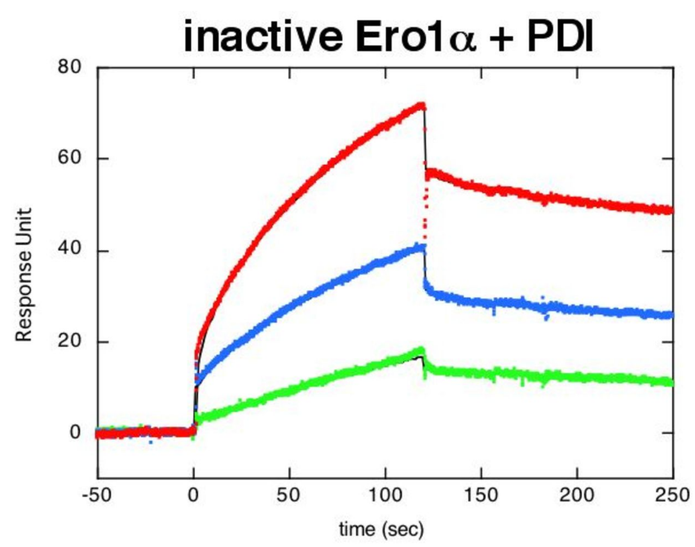

	k_{on} ($M^{-1}s^{-1}$)	k_{off} (s^{-1})	K_D (M)
hyperactive Ero1α	2.0±0.0 x10^3	4.1±0.2 x10^{-3}	2.1±0.1 x10^{-6}
inactive Ero1α	0.90±0.03 x10^3	6.9±0.3 x10^{-3}	7.7±0.6 x10^{-6}

Fig. 4 Inaba et al.

A

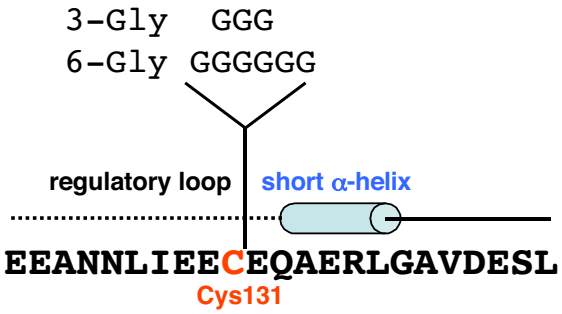

B

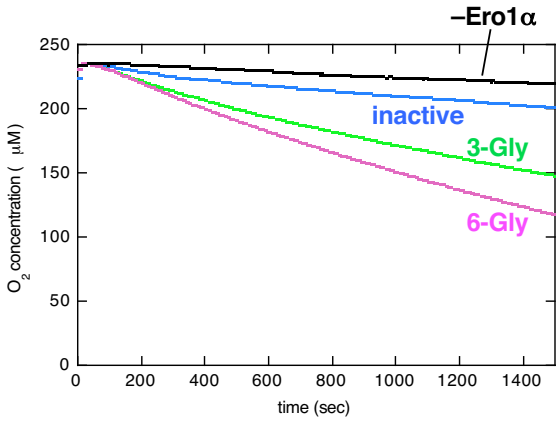

Fig. 5 Inaba et al.

A

PDI-based chimera

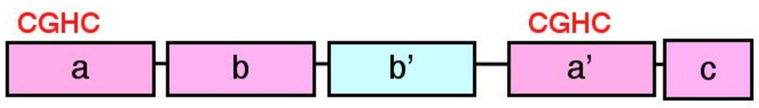

ERp57-based chimera

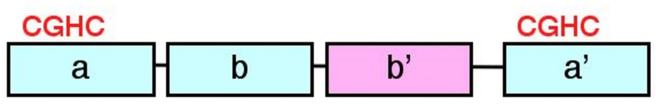

B

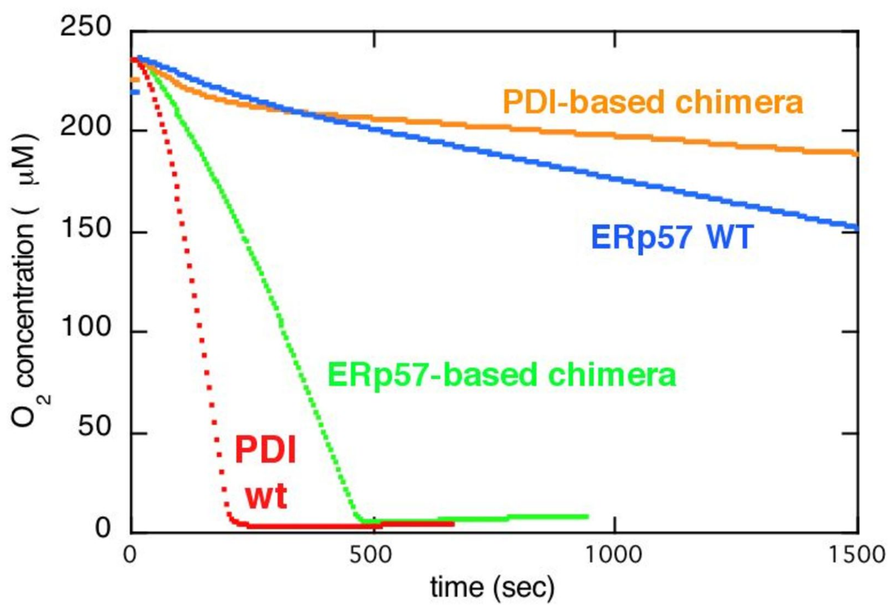

C

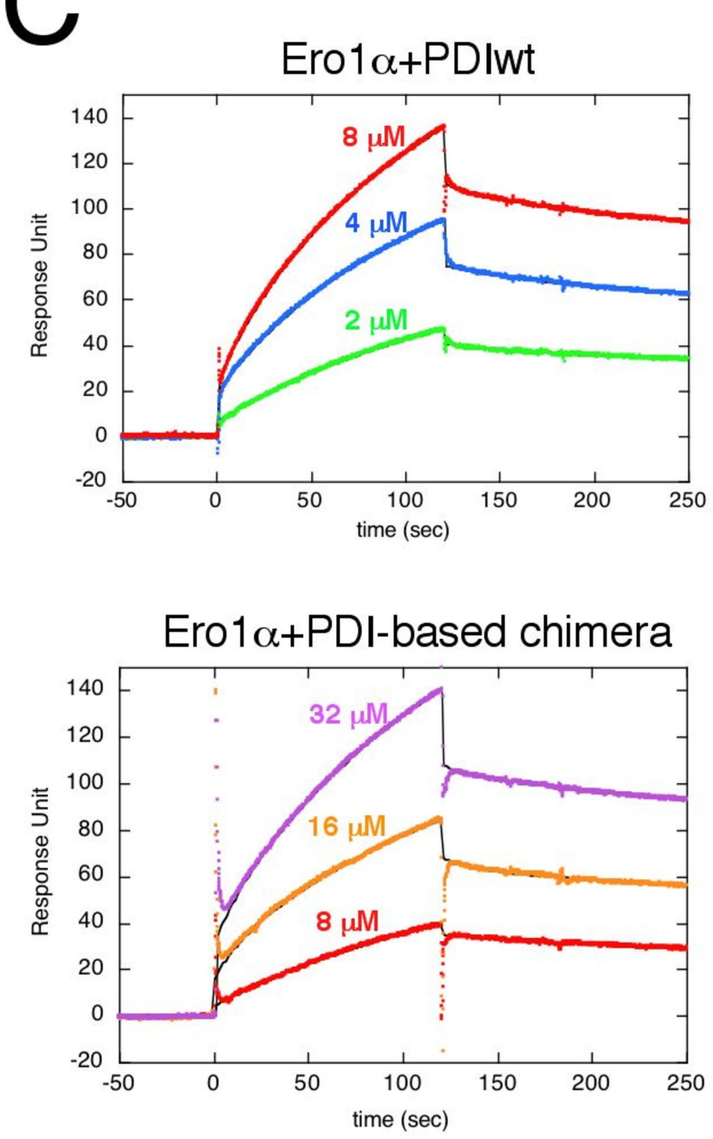

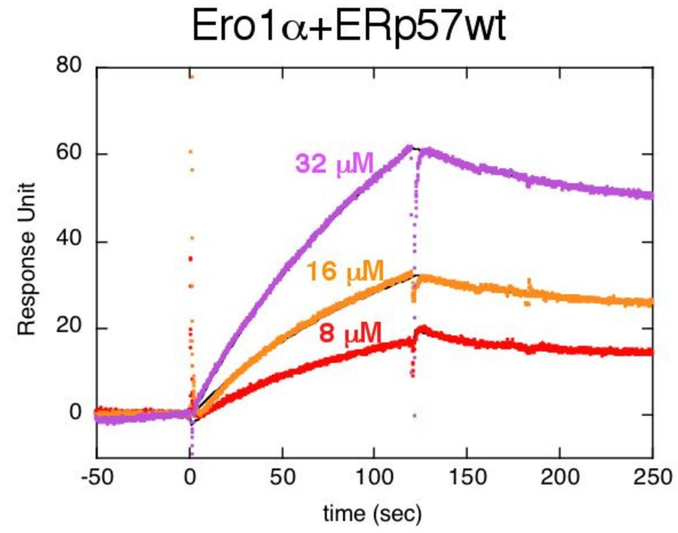

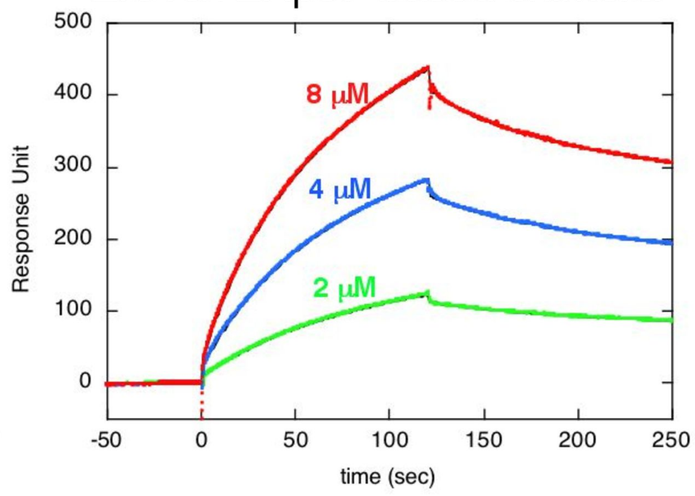

	k_{on} ($M^{-1}s^{-1}$)	k_{off} (s^{-1})	K_D (M)
PDI WT	2.0 ±0.0 x10^3	4.1±0.2 x10^{-3}	2.1±0.1 x10^{-6}
ERp57 WT	0.17±0.00 x10^3	3.2±0.1 x10^{-3}	19 ±1 x10^{-6}
PDI chimera	0.65±0.01 x10^3	29 ±1 x10^{-3}	45 ±2 x10^{-6}
ERp57 chimera	2.8 ±0.0 x10^3	11 ±0 x10^{-3}	3.8±0.0 x10^{-6}

Fig. 6 Inaba et al.

A

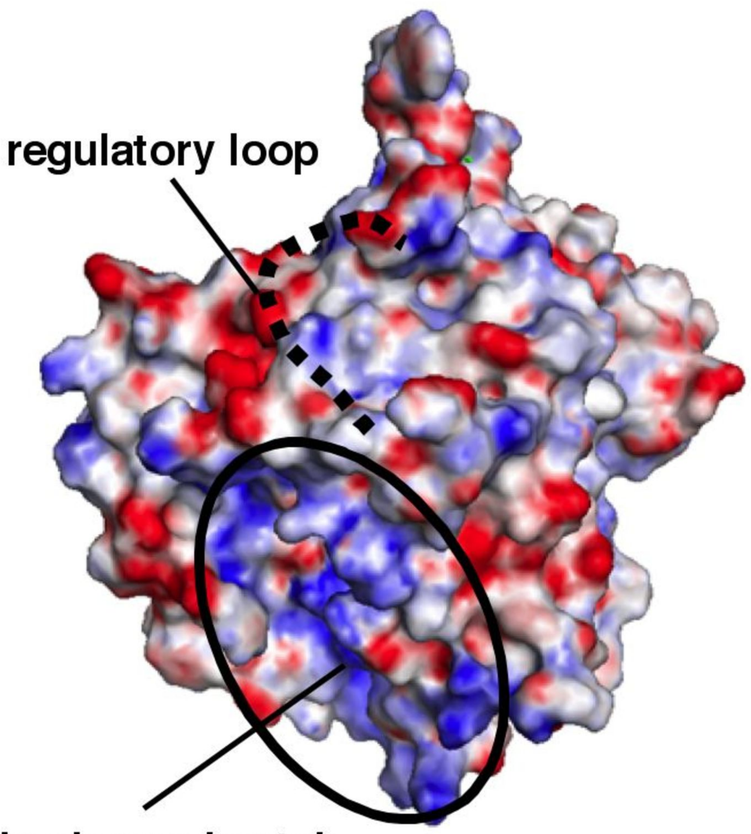

B

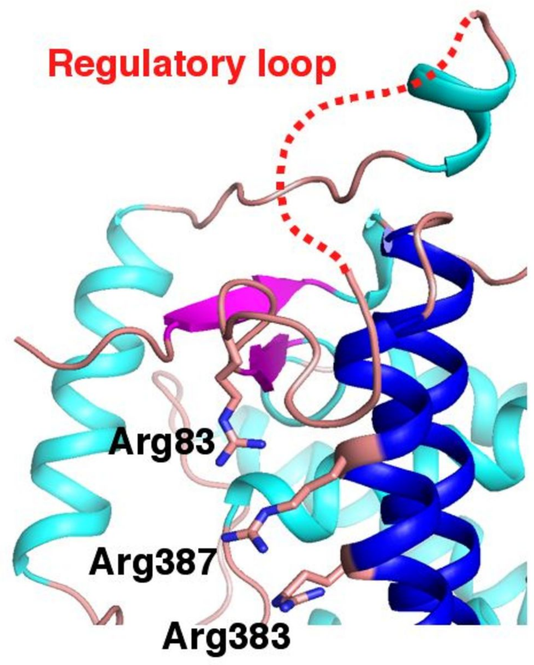

C

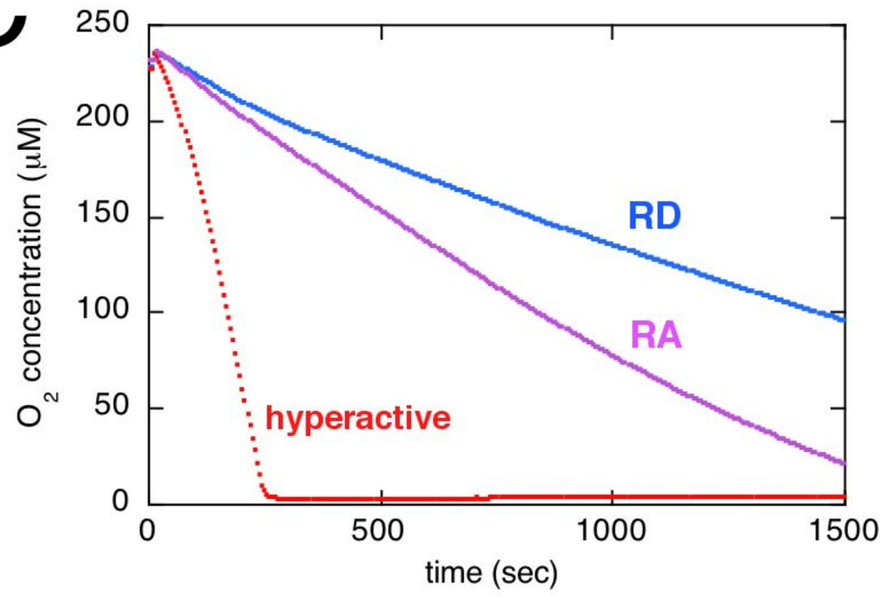

D

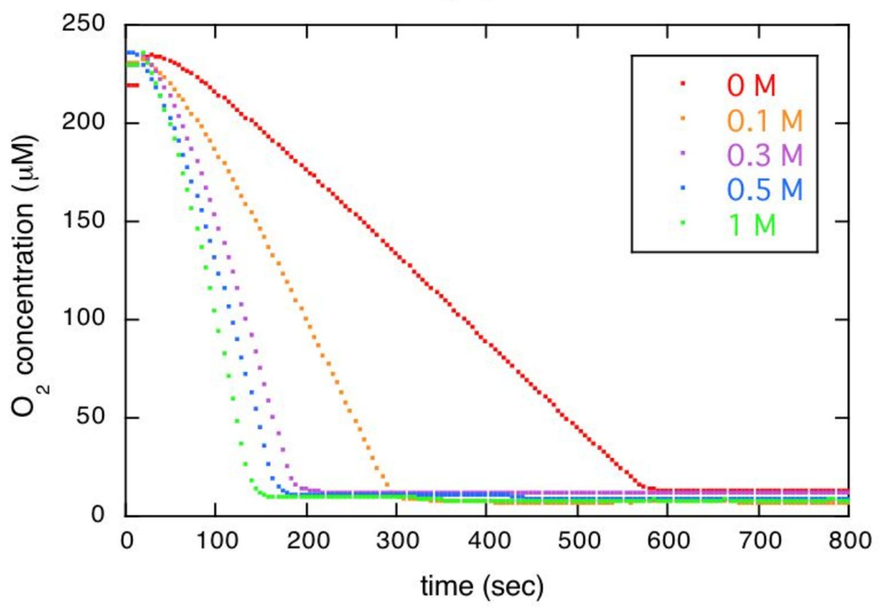

E

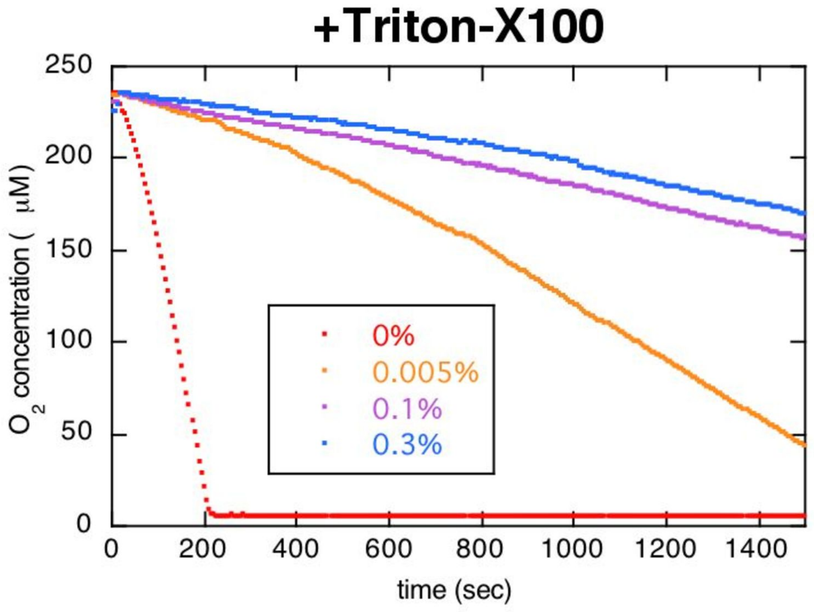

F

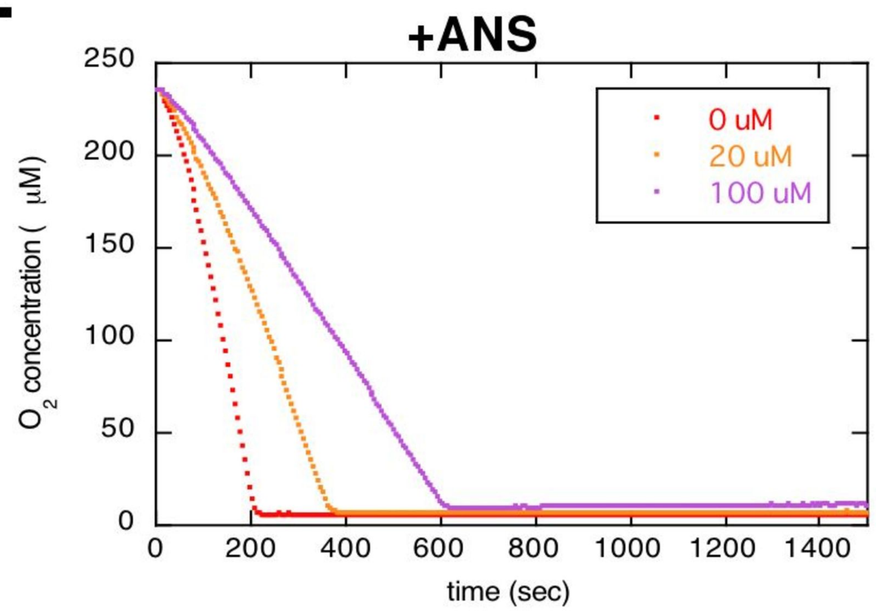

G

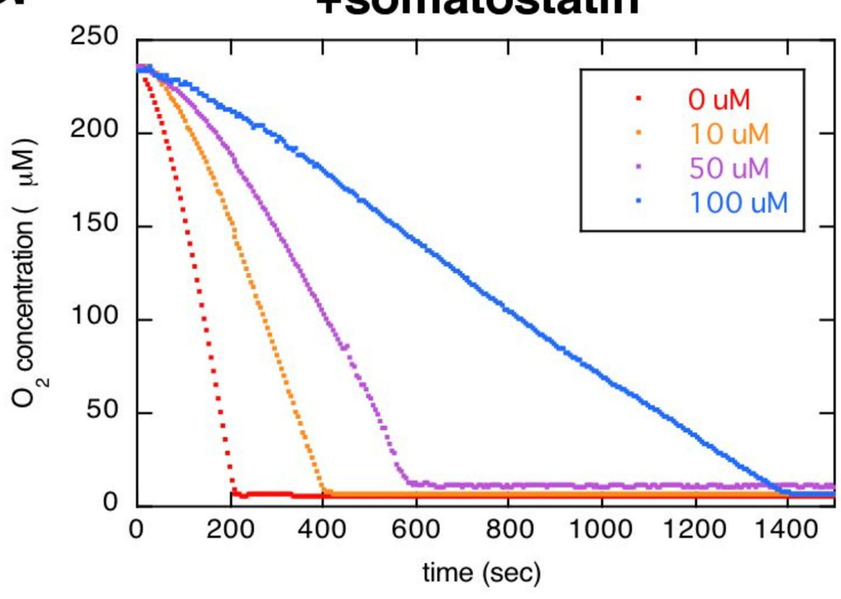

H

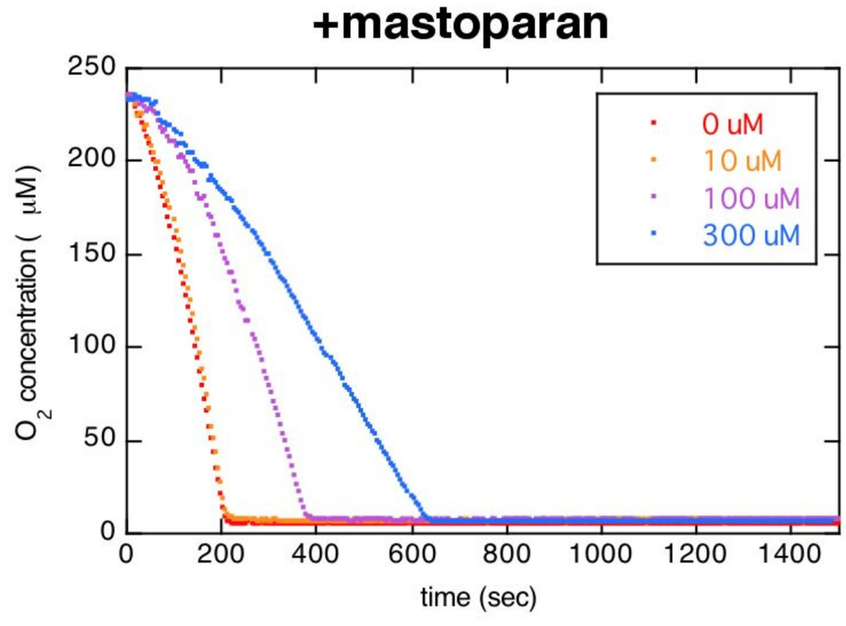

Fig. 7 Inaba et al.